

CoMFA and CoMSIA Analyses of *Pneumocystis carinii* Dihydrofolate Reductase, *Toxoplasma gondii* Dihydrofolate Reductase, and Rat Liver Dihydrofolate Reductase

Aleem Gangjee* and Xin Lin

Division of Medicinal Chemistry, Graduate School of Pharmaceutical Sciences, Duquesne University, Pittsburgh, Pennsylvania 15282

Received August 6, 2004

In a continuing effort to develop potent and selective dihydrofolate reductase (DHFR) inhibitors against opportunistic pathogens, we developed three-dimensional quantitative structure–activity relationship (3D QSAR) models for the inhibitory activity against *Pneumocystis carinii* (pc) DHFR, *Toxoplasma gondii* (tg) DHFR, and rat liver DHFR, using a data set of 179 structurally diverse compounds. To ensure a balanced distribution of more potent and less potent drugs in the training set, three different 90-compound training sets taken from the main data set were used, one for each enzyme, while the remaining 89 compounds in the main data set in each case were used as the test set. Three methods, namely, conventional CoMFA, all orientation search (AOS) CoMFA, and CoMSIA were applied to the training sets. While the AOS CoMFA models gave the best internal predictions (cross-validated r^2 values from the training sets), which are satisfactory, CoMSIA models gave the best external predictions (predictive r^2 values from the test sets). Both AOS CoMFA and CoMSIA analyses were used to construct stdev*coefficient contour maps which can be used to design new compounds in an interactive fashion.

Introduction

Infections caused by opportunistic pathogens *Pneumocystis carinii* (pc) and *Toxoplasma gondii* (tg) are the leading cause of morbidity and mortality in immunocompromised patients such as those with AIDS.¹ Dihydrofolate reductase (DHFR) inhibitors are the current drugs of choice for the treatment of these infections. Ideally, these drugs should efficiently reduce the growth of pathogenic cells via DHFR inhibition without affecting the essential functions of mammalian DHFR. Unfortunately, due to their lack of potency or selectivity, combinations of current DHFR inhibitors with other agents such as sulfa drugs are often required for synergistic effects or to prevent host toxicity, which leads to high costs. Despite these efforts, discontinuation of therapy is necessary in many cases as a result of severe side effects.^{2,3} Therefore, efforts continue to be directed toward the development of single agents which not only display high potency but are also selective against DHFR from *P. carinii* and/or *T. gondii* over mammalian DHFR, such as rat liver (rl) DHFR.^{4–7}

The discovery of clinically useful new DHFR inhibitors has proven to be a long and expensive task for individual researchers and the pharmaceutical industry alike. Thus, the ability to rationally design potent and selective DHFR inhibitors and narrow down the possible candidates has become crucial to the success of this endeavor. Computational techniques such as QSAR models can be used toward this end.

Most models for predicting DHFR inhibition in the current literature^{8–39} use homologous data sets of DHFR inhibitors with a specific heterocyclic core (e.g., quinazo-

lines, pyrimidines). As the numbers and structural diversities of active DHFR inhibitors increase, the formulation of a useful QSAR model becomes increasingly difficult. Mattioni et al.⁴⁰ recently developed QSAR models that correlated chemical structure and inhibition potency for three types of DHFR: rl, pc, and tg. The results, however, did not give structural information about the binding sites. Thus, there is a dearth of information regarding molecular models of pcDHFR and tgDHFR that not only predict novel biologically active compounds but also provide pharmacophores that could be used as a guide for future drug design.

In this paper, we report the development of 3D QSAR models that correlate the 3D chemical structures of 179 compounds reported from our laboratory and their^{41–53} inhibitory potencies for pcDHFR, tgDHFR, and rlDHFR. For the inhibitory activity against each enzyme, three 3D QSAR models were developed using the conventional comparative molecular field analysis (CoMFA), a modified routine of CoMFA known as all-orientation search (AOS), and comparative molecular similarity indices analysis (CoMSIA), respectively. The goal of this work is to build robust 3D QSAR models to predict the inhibition values for a larger, more diverse DHFR data set, which is composed of different classes of inhibitors with some relatively newly developed DHFR inhibitors.

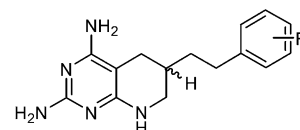
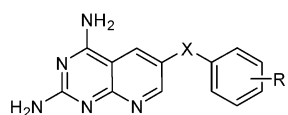
Computational Details

1. Data Set and Biology Activity. To ensure that all experimental values are the results of consistent assay conditions, the training sets and test sets for the analyses were taken from a data set consisting of 179 compounds designed, synthesized, and reported by Gangjee et al.^{41–53} with the IC₅₀ values (μM) of its compounds against pcDHFR, tgDHFR, and rlDHFR determined by Queener et al. The structures and IC₅₀ values of the compounds are listed in Table 1.

* Tel: 412-396-6070. Fax: 412-396-5593. E-mail: gangjee@duq.edu.

Table 1. Structures and IC₅₀ Values of the Compounds Used in Developing the Models

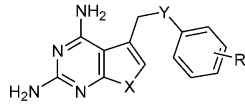
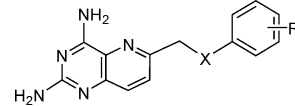
Cmpd	R1	R2	R3	Pc	tg	rl	Ref	Cmpd	R1	R2	R3	pc	tg	rl	Ref
1	CH ₃	H	3',4',5'-(OCH ₃) ₃	0.086	0.0074	0.0021	41	14	CH ₃	CH ₃	2',4'-(OCH ₃) ₂	0.51	0.038	0.33	41
2	CH ₃	CH ₃	3',4',5'-(OCH ₃) ₃	0.0132	0.00058	0.0076	41	15	CH ₃	CH ₃	3',4'-(OCH ₃) ₂	0.32	0.029	0.044	41
3	CH ₃	CHO	3',4',5'-(OCH ₃) ₃	0.55	0.013	0.11	41	16	CH ₃	H	3',4'-(OCH ₃) ₂	0.044	0.0088	0.0076	41
4	CH ₃	H	3',4'-Cl ₂	0.32	0.028	0.053	41	17	CH ₃	H	2',4'-(OCH ₃) ₂	0.316	0.0565	0.214	41
5	CH ₃	CHO	3',4'-Cl ₂	0.51	0.083	0.14	41	18	CH ₃	H	3',5'-(OCH ₃) ₂	0.0229	0.0048	0.0425	41
6	CH ₃	CH ₃	3',4'-Cl ₂	0.1	0.027	0.042	41	19	CH ₃	CH ₃	3',5'-(OCH ₃) ₂	0.13	0.058	0.17	41
7	CH ₃	H	3',4',5'-Cl ₃	0.063	0.012	0.033	41	20	CH ₃	H	2',3'-(CH) ₄ -4'- OCH ₃	0.041	0.023	0.054	41
8	CH ₃	CHO	3',4',5'-Cl ₃	0.52	0.094	0.25	41	21	CH ₃	CH ₂ C≡CH	3',4',5'-(OCH ₃) ₃	0.0535	0.0077	0.0118	41
9	CH ₃	H	2',3'-(CH) ₄	0.573	0.0145	0.0296	41	22	CH ₃	CH(CH ₃) ₂	3',4',5'-(OCH ₃) ₃	0.0134	0.0067	0.0175	41
10	CH ₃	H	2',5'-(OCH ₃) ₂	0.046	0.016	0.128	41	23	CH ₃	CH ₂ CH ₃	3',4',5'-(OCH ₃) ₃	0.497	0.0027	0.0105	41
11	CH ₃	CH ₃	2',5'-(OCH ₃) ₂	0.216	0.0301	0.407	41	24	H	H	3',4',5'-(OCH ₃) ₃	1.5	0.3	1.9	41
12	CH ₃	H	2',5'- (OCH ₂ CH ₃) ₂	0.0767	0.017	0.0174	41	25	H	CH ₃	3',4',5'-(OCH ₃) ₃	0.24	0.009	0.28	41
13	CH ₃	CH ₃	2',5'- (OCH ₂ CH ₃) ₂	3.1	0.1	3	41	26	H	CH ₂ CH ₃	3',4',5'-(OCH ₃) ₃	0.19	0.049	0.12	41



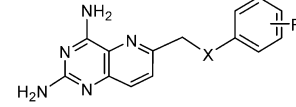
Cmpd	X	R	pc	tg	rl	Ref.	Cmpd	R	pc	tg	rl	Ref
27	CH=CH	3',4'-(OCH ₃) ₂	2.6	1.4	2.1	42	32	3',4',5'-(OCH ₃) ₃	61.7	0.47	6.1	42
28	CH=CH	4'-OCH ₃	5.3	1.5	11.8	42	33	3',4',5'-(OCH ₃) ₃	7.7	1.1	2.1	42
29	CH ₂ CH ₂	3',4',5'-(OCH ₃) ₃	5	0.2	1.14	42						
30	CH ₂ CH ₂	3',4'-(OCH ₃) ₂	1.4	0.2	0.61	42						
31	CH ₂ CH ₂	4'-OCH ₃	0.29	0.25	0.26	42						

Cmpd	pc	tg	rl	Ref
34	18.5	1.1	7.4	42

Table 1 (Continued)

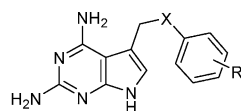



Cmpd	X	Y	R	pc	tg	rl	Ref	Cmpd	X	R	pc	tg	rl	Ref
35	NH	NH	4'-OCH ₃	279	6	63	43	48	NH	3',4'-Cl ₂	0.41	0.057	0.054	45
36	NH	NH	2',5'- (OCH ₃) ₂	45.7	1.7	156	43	49	NH	3',4'-(CH) ₄	1.6	0.16	0.21	45
37	NH	NH	3',4'-Cl ₂	35.3	1.4	14.4	43	50	NH	3',4'- (OCH ₃) ₂	0.9	0.09	0.06	45
38	NH	NH	2',3'-(CH) ₄	307	1.1	59.3	43	51	NH	3'-Cl	2	0.13	0.14	45
39	NH	NH	3',4'- (OCH ₃) ₂	119	4.3	116	43	52	NH	3'-OCH ₃	1.7	0.1	0.2	45
40	O	S	2',3'-(CH) ₄	19	19	23	44	53	NH	2'-OCH ₃	2.7	0.12	0.42	45
41	O	NH	2',3'-(CH) ₄	13.5	37	12	44	54	NH	2'-Cl	0.53	0.11	0.14	45
42	O	NH	3',4'-(CH) ₄	41	38	36.5	44	55	NH	3',4',5'- (OCH ₃) ₃	2	0.04	0.2	45
43	O	NH	2'-C ₆ H ₅	7.7	45.4	137	44	56	NCH ₃	4'-OCH ₃	0.25	0.016	0.018	45
44	O	NH	4'-OC ₆ H ₅	8.1	32.4	16.2	44	57	NH	H	1.7	0.085	0.26	45
45	O	NCH ₃	3',4'-(CH) ₄	14.8	23.6	14.6	44	58	NH	3',4',5'-Cl ₃	0.66	0.087	0.044	45
46	O	S	3',4'-(CH) ₄	0.65	11.6	12.3	44	59	NH	2',6'-Cl ₂	1	0.028	0.082	45
47	O	NCH ₃	3',4',5'-Cl ₃	284	21.5	34.3	44	60	NH	4'-OCH ₃	0.85	0.054	0.073	45

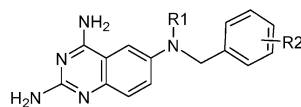


Cmpd	X	R	pc	tg	rl	Ref	No	X	R	pc	tg	rl	Ref
61	NCH ₃	2',5'-(OCH ₃) ₂	0.21	0.025	0.05	46	73	NCH ₃	2',4'-Cl ₂	0.5	0.05	0.058	45
62	NH	2',5'-(OCH ₃) ₂	4.4	0.12	0.28	45	74	NH	2',5'-Cl ₂	1.6	0.091	0.2	45
63	NH	2',4',6'-Cl ₃	2	0.046	0.57	45	75	NCH ₃	2',5'-Cl ₂	0.15	0.025	0.047	45
64	NCH ₃	3',4'-(OCH ₃) ₂	0.091	0.0098	0.0027	45	76	NCH ₃	2'-Cl	0.21	0.015	0.12	45
65	NCH ₃	2',4'-(OCH ₃) ₂	0.16	0.014	0.016	45	77	NCH ₃	2',6'-Cl ₂	0.17	0.03	0.048	45
66	NCH ₃	3'-OCH ₃	0.097	0.015	0.035	45	78	NCH ₃	3',4',5'-(OCH ₃) ₃	0.12	0.044	0.052	45
67	NCH ₃	3',4'-(CH) ₄	0.052	0.016	0.0072	45	79	S	H	2	0.13	0.52	45
68	NCH ₃	2',3'-(CH) ₄	0.04	0.018	0.0073	45	80	NH	2',4'-Cl ₂	0.73	0.05	0.088	45
69	NCH ₃	2'-OCH ₃	0.51	0.026	0.12	45	81	S	2',3'-(CH) ₄	0.47	0.049	0.16	45
70	NCH ₃	3',4'-Cl ₂	0.038	0.027	0.017	45	82	S	3',4'-(CH) ₄	0.38	0.048	0.086	45
71	NCH ₃	H	0.29	0.0084	0.024	45	83	NH	2',3'-(CH) ₄	0.23	0.026	0.04	45
72	NCH ₃	3',4',5'-Cl ₃	0.25	0.038	0.087	45	84	NH	2',4'-(OCH ₃) ₂	5.5	0.14	0.32	45

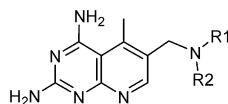
Table 1 (Continued)



Cmpd	X	R	pc	tg	rl	Ref	Cmpd	X	R	pc	Tg	rl	Ref
85	NCH ₃	3',4'-Cl ₂	28.3	1	3	46	88	S	3',4'-(OCH ₃) ₂	11.1	2.6	16.7	46
86	NCH ₃	2',3'-(CH) ₄	209	0.87	8.2	46	89	S	2',3'-(CH) ₄	10.6	0.81	3	46
87	S	3',4'-Cl ₂	58.5	11.6	5.3	46	90	S	3',4'-(CH) ₄	929	9.2	82.9	46



Cmpd	R1	R2	pc	tg	rl	Ref	Cmpd	R1	R2	pc	Tg	rl	Ref
91	H	3',4',5'-(OCH ₃) ₃	6.8	0.084	0.9	47	98	CH ₃	2',4',6'-(OCH ₃) ₃	116	0.95	22.7	47
92	H	2',5'-(OCH ₃) ₂	4.6	0.16	1.1	47	99	CH ₃	2',3',4'-(OCH ₃) ₃	0.052	0.017	0.019	47
93	H	3',5'-(OCH ₃) ₂	2.2	0.12	0.84	47	100	H	2',3'-(CH) ₄	0.72	0.099	0.19	47
94	H	H	8.7	0.32	0.66	47	101	H	2',4',5'-(OCH ₃) ₃	5.4	0.124	1.6	47
95	H	2',4'-(OCH ₃) ₂	4.4	0.17	1.2	47	102	CH ₃	2',3'-(CH) ₄	0.017	0.021	0.017	47
96	H	2',3',4'-(OCH ₃) ₃	4.9	0.19	1.3	47	103	CH ₃	2',5'-(OCH ₃) ₂	0.087	0.03	0.026	47
97	CH ₃	3',5'-(OCH ₃) ₂	0.0238	0.0093	0.0082	48	104	CH ₃	2',4'-(OCH ₃) ₂	0.1	0.039	0.043	48



Cmpd	R1	R2	pc	tg	rl	Ref	Cmpd	R1	R2	Pc	tg	rl	Ref
105	H	3'-ClC ₆ H ₄	0.023	0.011	0.037	49	119	H		0.41	0.049	0.23	50
106	H	4'-ClC ₆ H ₄	0.0554	0.019	0.051	49	120	H		0.57	0.077	0.47	50
107	H	2'-ClC ₆ H ₄	0.047	0.0071	0.088	49	121	H		0.85	0.11	0.13	50
108	H	4'-OCH ₃ C ₆ H ₄	0.0954	0.012	0.0556	49	122	H		0.35	0.033	0.23	50
109	H	2'-OCH ₃ C ₆ H ₄	0.117	0.023	0.169	49	123	H		1.8	0.6	3.5	50
110	H	4'-BrC ₆ H ₄	0.0808	0.0095	0.0349	49	124	H		0.62	0.075	0.17	49
111	CH ₃	4'-OCH ₃ C ₆ H ₄	0.035	0.0073	0.013	49	125	H		0.064	0.068	0.44	49
112	CH ₃	C ₆ H ₅	0.03	0.0063	0.018	49							
113	CH ₃	4'-ClC ₆ H ₄	0.08	0.0017	0.17	49							
114	CH ₃	4'-ClC ₆ H ₄	0.029	0.0054	0.026	49							
115	CH ₃	4'-BrC ₆ H ₄	0.037	0.03	0.036	48							
116	H	2'-OCH ₃ C ₆ H ₄	0.0689	0.0074	0.0801	48							

Table 1 (Continued)

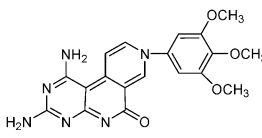
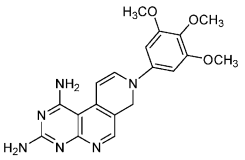
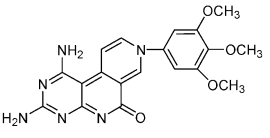
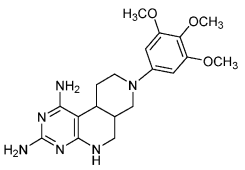
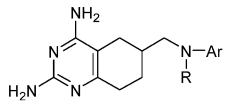
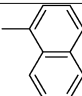
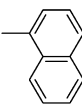
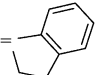
Cmpd	pc	tg	rl	Ref.	No.	pc	tg	rl	Ref.				
	4.28	0.24	1.12	50	126		4.6	0.76	0.47	50			
	2.4	0.052	0.086	50	127		2.2	0.29	0.16	50			
													
Cmpd	R	Ar	pc	tg	rl	Ref.	Cmpd	R	Ar	Pc	tg	rl	Ref.
130	H		0.517	0.036	0.139	51	140	H	2',5'-(OC ₂ H ₅) ₂ C ₆ H ₃	1.57	0.14	1.47	51
131	CH ₃		0.1	0.023	0.047	51	141	H	2',5'-Cl ₂ C ₆ H ₃	0.41	0.097	0.24	51
132	CH ₃	3',4',5'- (OCH ₃) ₃ C ₆ H ₂	0.095	0.007	0.038	51	142	H	4'-ClC ₆ H ₄	0.94	0.078	0.128	51
133	H	3',4'-Cl ₂ C ₆ H ₃	6.8	0.11	0.15	51	143	R, Ar =		0.21	0.027	0.16	51
134	CH ₃	3',4'-Cl ₂ C ₆ H ₃	0.246	0.021	0.034	51	144	CH ₃	-CH ₂ -3',4',5'- (OCH ₃) ₃ C ₆ H ₂	3.1	0.33	1.63	51
135	H	3',4',5'- (OCH ₃) ₃ C ₆ H ₂	4.6	0.054	0.29	51	145	CH ₃	2',5'-(OCH ₃) ₂ C ₆ H ₃	0.3	0.015	0.26	51
136	H	3'-BrC ₆ H ₄	0.33	0.03	0.227	51	146	CH ₃	4'-ClC ₆ H ₄	0.171	0.022	0.067	51
137	H	2',6'-Cl ₂ C ₆ H ₃	0.502	0.0099	0.109	51	147	C ₂ H ₅	2',5'-(OCH ₃) ₂ C ₆ H ₃	0.114	0.017	0.071	51
138	CH ₃	2',5'-(OC ₂ H ₅) ₂ C ₆ H ₃	0.319	0.017	0.116	51	148	CH ₂ C≡C H	3',4',5'-(OCH ₃) ₃ C ₆ H ₂	0.119	0.012	0.074	51
139	H	2',5'-(OCH ₃) ₂ C ₆ H ₃	1.67	0.181	0.56	51	149	H	3',4',5'-(OCH ₃) ₃ C ₆ H ₂	4.6	0.054	0.29	51

Table 1 (Continued)

Cmpd	X	R	pc	tg	rl	Ref	Cmpd	X	R	pc	tg	rl	Ref
150	S	2'-OCH ₃	2.2	0.058	0.23	52	156	NH	3',4'-(OCH ₃) ₂	40.4	0.68	1.1	52
151	S	4'-OCH ₃	0.7	0.045	0.075	52	157	NH	2',5'-(OCH ₃) ₂	16.1	0.73	3.6	52
152	S	3',4'-(OCH ₃) ₂	0.086	0.019	0.018	52	158	NH	3',4',5'-(OCH ₃) ₃	25.9	2.4	3.2	52
153	SO ₂	2'-OCH ₃	3.2	0.21	1.4	52	159	NH	H	8.3	0.3	0.43	52
154	NH	2'-OCH ₃	8.7	0.46	0.26	52	160	NH	4'-Cl	14.6	0.83	0.82	52
155	NH	4'-OCH ₃	90.4	2.8	3.8	52							

Cmpd	n	R1	R2	R3	pc	tg	rl	Ref	Cmpd	n	R1	R2	R3	pc	tg	rl	Ref
161	0	CH ₃	H	H	0.068	0.032	0.14	53	171	0	CH ₃	H	2',3',4'-(OCH ₃) ₃	0.079	0.026	0.03	52
162	1	CH ₃	H	H	1.8	0.92	1.4	52	172	0	H	H	3',4'-(OCH ₃) ₂	4.8	0.73	1.5	52
163	0	CH ₃	H	2',5'-(OCH ₃) ₂	0.084	0.0063	0.057	53	173	0	CH ₃	H	3',5'-(OCH ₃) ₂	0.076	0.031	0.072	52
164	0	H	H	2',3',4'-(OCH ₃) ₃	14.1	0.35	3.3	52	174	0	H	H	3',5'-(OCH ₃) ₂	5.7	1.2	3.4	52
165	0	H	H	2',4',5'-(OCH ₃) ₃	5.5	0.48	1.1	52	175	0	H	H	2',3'-(CH) ₄	3.9	0.98	0.24	52
166	0	H	H	3',4',5'-(OCH ₃) ₃	14.1	0.35	3.3	52	176	0	H	H	4'-OCH ₃ -2',3'-(CH) ₄	8.2	0.38	0.43	52
167	0	CH ₃	H	3',4',5'-(OCH ₃) ₃	0.061	0.014	0.033	52	177	0	H	H	H	2.7	0.52	2.1	52
168	0	H	H	2',5'-(OCH ₃) ₂	3.8	0.31	0.35	52	178	0	H	CH ₃	3',4',5'-(OCH ₃) ₃	9.2	0.194	1.27	52
169	0	H	H	2',4',6-(OCH ₃) ₃	20.7	0.23	1.2	52	179	1	H	H	H	1.94	4.45	0.28	52
170	0	H	H	4'-OC ₆ H ₅	24.3	3.7	2.9	52									

One goal of this study was to test the predictability of the analyses. For each enzyme, we divided the compounds into a training set containing 90 compounds and a test set of 89 compounds in order to assess the predictive power of the model. These sets contained compounds from all structural families and represented a balanced number of both the more active and the less active compounds.

2. Structure Alignment. The most critical requirement in 3D QSAR is the alignment of all compounds according to a suitable conformational template. Compound **46** (Table 1) was reported by Gangjee et al.⁴⁴ as the third most selective

pcDHFR inhibitor known to date; its low energy conformation taken from the crystal structure with pcDHFR was chosen as the template for the alignment (Figure 1).

To ensure a successful analysis, the aligned compounds should not only adopt similar spatial orientations but also assume comparable conformations. The "flexible alignment" method⁵⁵ implemented by the Molecular Operating Environment (MOE) suite⁵⁶ is a molecular alignment approach that meets both requirements. Thus all compounds were aligned pairwise against the template using the "flexible alignment" approach. Atomic coordinates of the template were fixed during

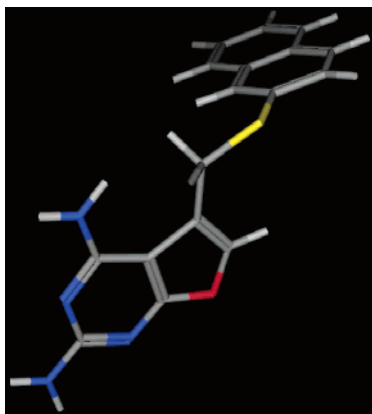


Figure 1. The low-energy conformation of the template molecule **46**.

the alignment, MMFF94 was chosen as the force field, and the following chemical features were selected during the flexible alignment search: molecular volume, H-bond acceptor, H-bond donor, acidic and basic function. For each analyzed compound, conformers with the best fitness score (calculated in MOE) were selected to be analyzed with CoMFA, AOS, and CoMSIA in SYBYL.⁵⁷ A Scientific Vector Language (SVL) script was written to accomplish the above tasks in MOE automatically.

The resulting aligned structures were imported into a Sybyl molecular database without further energy minimization. Charge calculations were done using the Gasteiger–Huckel method as implemented in Sybyl.

As mentioned in the Data Set and Biology Activity section, for the analysis of inhibitory activity against each enzyme, the above molecular database was split into a training set database containing 90 compounds and a test set database containing 89 compounds.

3.1. Conventional CoMFA. CoMFA was performed using the QSAR module in Sybyl 6.7. For each training set compound the CoMFA descriptors, steric (Lennard-Jones 6-12 potential) and electrostatic (Coulombic potential) field energies, were calculated using the SYBYL default parameters. The CoMFA region was defined to extend beyond the van der Waals envelopes of all molecules by 4.0 Å along the principal axes of the Cartesian coordinate system. A distance dependent dielectric constant was used. An sp³ carbon atom with +1.0 charge served as the probe atom to calculate steric and electrostatic fields. The steric and electrostatic contributions were truncated at 30 kcal/mol, and electrostatic contributions were dropped at lattice intersections with maximum steric interactions. The CoMFA steric and electrostatic fields generated were scaled by the CoMFA standard option in SYBYL.

3.2. All-Orientation Search (AOS) CoMFA. As first reported by Cho et. al,⁵⁸ the cross-validated r^2 (q^2) value of CoMFA analysis, which serves as a quantitative measure of the predictivity, fluctuates with the orientation of the aligned molecular aggregate on the computer screen by up to 0.5 q^2 unit. The reason for this fluctuation in q^2 values lies in the fact that conventional CoMFA samples the continuous molecular field at discrete lattice points and calculates the steric and electrostatic field energies on each lattice point with distance-sensitive functions, such as the Lennard-Jones 6-12 potential. When the molecular aggregate rotates, so does the molecular field surrounding the aggregate. The lattice box in CoMFA, however, is always axis-aligned and does not rotate along with them. Thus, different points in the same molecular field will be mapped onto the lattice points resulting in different field energy values. These values, when processed subsequently by partial least squares (PLS) to produce the final model, will cause a variation in the q^2 value and, hence, the predictivity of the model.

The AOS routine⁵⁴ optimizes the field sampling by rotating the molecular aggregate systematically and picking the orientation that produces the highest q^2 value. The details of the

AOS routine were described previously.⁵⁴ Briefly, the whole aggregate was rotated about the x , y , and z axes systematically with an increment of 30° using the STATIC ROTATE command. For each orientation, a conventional CoMFA was performed as described above and the predictive value of the model was evaluated using leave-one-out (LOO) cross-validation with sample-distance partial least squares (SAMPLS). The orientation that gave the highest q^2 value was selected to produce the final model. A Sybyl Programming language (SPL) script was written to perform the AOS routine as described⁵⁴ automatically.

3.3. CoMSIA. CoMSIA analysis was also performed using the QSAR module in Sybyl 6.7. The five similarity indices in CoMSIA (steric, electrostatic, hydrophobic, H-bond donor, and H-bond acceptor descriptors) were calculated⁵⁹ using a probe atom with a radius of 1 Å and a +1.0 charge placed at the lattice points of the same region box as was used for the conventional CoMFA calculations; CoMSIA similarity indices (A_F) for a molecule j with atoms i at a grid point q are calculated by eq 1,

$$A_{F,K}^q(j) = -\sum \omega_{\text{probe},k} \omega_{ik} e^{-\alpha r_{iq}^2} \quad (1)$$

where k represents the following physicochemical properties: steric, electrostatic, hydrophobic, H-bond donor, and H-bond acceptor. A Gaussian type distance dependence was used between the grid point q and each atom i of the molecule. The default value of 0.3 was used as the attenuation factor (α). Here, steric indices are related to the third power of the atomic radii, electrostatic descriptors are derived from atomic partial charges, hydrophobic fields are derived from atom-based parameters,⁶⁰ and H-bond donor and acceptor indices are obtained by a rule-based method based on experimental results.⁶¹

4. PLS Analysis. The conventional CoMFA, AOS CoMFA, and CoMSIA descriptors derived above were used as explanatory variables, and pIC₅₀ ($-\log \text{IC}_{50}$) values were used as the target variable in PLS regression analyses to derive 3D QSAR models using the implementation in the SYBYL package. The predictive value of the models was evaluated by leave-one-out (LOO) cross-validation with SAMPLS. The cross-validated coefficient, q^2 , was calculated using eq 2,

$$q^2 = 1 - \frac{\sum (Y_{\text{pred}} - Y_{\text{actual}})^2}{\sum (Y_{\text{actual}} - Y_{\text{mean}})^2} \quad (2)$$

where Y_{pred} , Y_{actual} , and Y_{mean} are predicted, actual, and mean values of the target property (pIC₅₀), respectively. $\sum (Y_{\text{pred}} - Y_{\text{actual}})^2$ is the predictive sum of squares (PRESS). The number of components giving the lowest PRESS value or the optimal number of components (ONC) was used to generate the final PLS regression models. The conventional correlation coefficient r^2 and its standard error, s , were subsequently computed for the final PLS models. CoMFA and CoMSIA coefficient maps were generated by interpolation of the pairwise products between the PLS coefficients and the standard deviations of the corresponding CoMFA or CoMSIA descriptor values.

5. Results and Validation. 5.1. CoMFA Analysis. For each enzyme, a unique set of 90 DHFR inhibitors that had a balanced distribution of more active and less active compounds against the specific enzyme among each class was chosen from the main data set composed of the 179 flexible-aligned antifolates (Figure 2) to derive both the conventional and the AOS CoMFA models, and the remaining 89 compounds were used as the test set. Thus, a total of six models, two for pDHFR, tgDHFR, and rDHFR, respectively, were generated. The key statistical parameters associated with these models are shown in Table 2. The predicted pIC₅₀ values for pDHFR, tgDHFR, and rDHFR training set compounds and the residual values are given in Tables 3, 4, and 5, respectively. AOS CoMFA showed better correlation than conventional CoMFA. For the

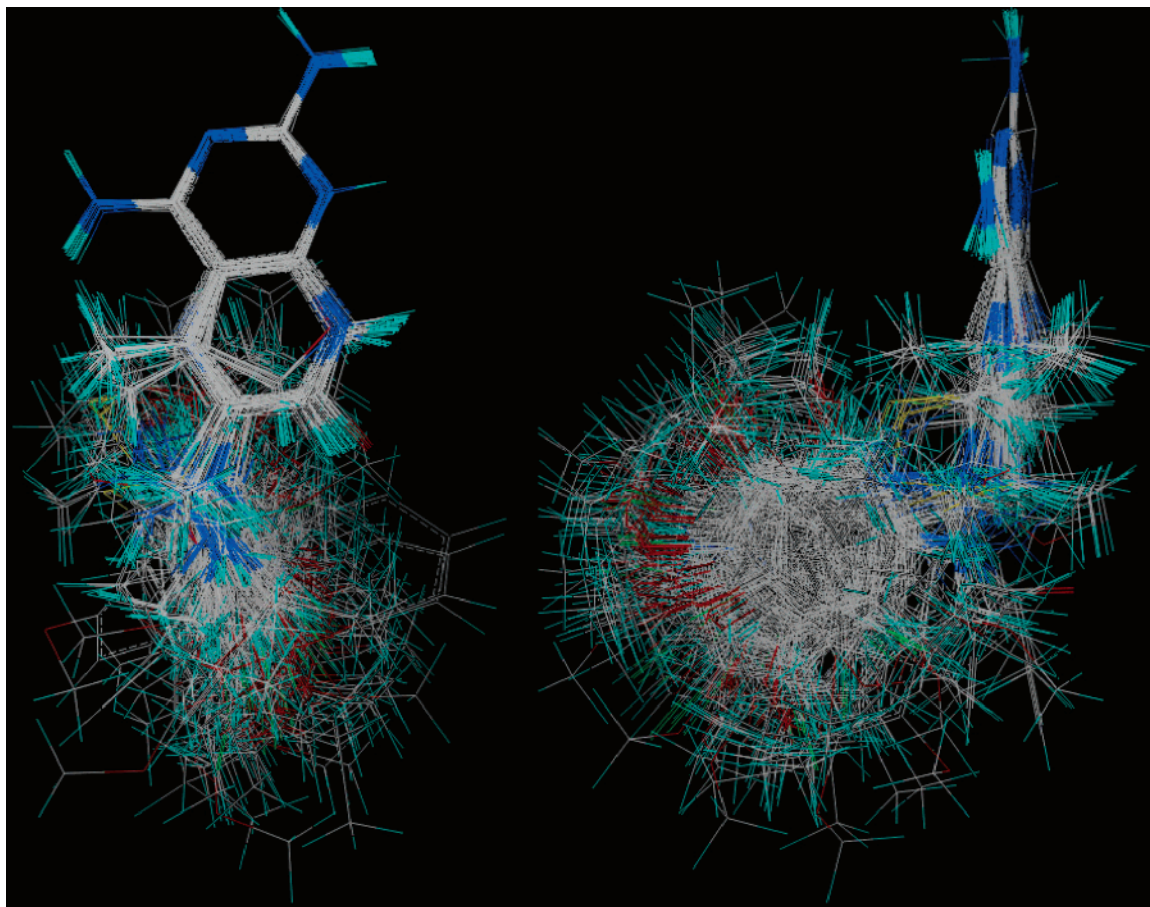


Figure 2. Orthographic view of the aligned 179 compounds.

Table 2. Statistical Data for QSAR Method Results

	pc			tg			rl		
	CoMFA	AOS	CoMSIA	CoMFA	AOS	CoMSIA	CoMFA	AOS	CoMSIA
CV- r^2 (q^2)	0.402	0.604	0.542	0.366	0.600	0.461	0.477	0.634	0.475
optimal no. of components	5	5	3	6	10	7	6	6	2
std error	0.429	0.363	0.505	0.379	0.184	0.306	0.352	0.257	0.549
non-CV- r^2	0.829	0.878	0.758	0.853	0.967	0.905	0.886	0.939	0.708
F value	81.416	120.667	89.713	79.964	231.394	111.766	107.046	213.094	105.585
contributions									
steric	0.524	0.533	0.074	0.525	0.471	0.072	0.535	0.482	0.072
electrostatic	0.476	0.467	0.296	0.475	0.529	0.359	0.465	0.518	0.283
H-bond donor			0.093			0.093			0.123
H-bond acceptor			0.157			0.133			0.146
hydrophobic			0.380			0.343			0.376
predictive r^2	0.438	0.461	0.544	0.490	0.505	0.648	0.337	0.421	0.488

pcDHFR training set, AOS significantly improved the cross-validated r^2 (q^2) from 0.402 (ONC = 5) to 0.604 (ONC = 5). AOS also reduced the average absolute residual value from 0.32 for conventional CoMFA to 0.28. For the tgDHFR training set, AOS significantly improved the q^2 value from 0.366 (ONC = 6) to 0.600 (ONC = 10). AOS also significantly reduced the average absolute residual value from 0.29 for conventional CoMFA to 0.12. For the rat liver DHFR training set as well as AOS significantly improved q^2 from 0.477 (ONC = 6) to 0.634 (ONC = 6). AOS also reduced the average absolute residual value from 0.12 for conventional CoMFA to 0.10. A $q^2 \geq 0.5$ is generally considered as an indication that the model is internally predictive, thus the q^2 values obtained in the present case imparted reliability to our AOS CoMFA models.

To validate our models, we attempted to predict the inhibitory activity against pcDHFR, tgDHFR, and rIDHFR for the 89 compounds in each corresponding test set. The predicted r^2 values were obtained and are shown in Table 2. The predicted pIC₅₀ values for pcDHFR, tgDHFR, and rIDHFR test

set compounds as well as the residual values are given in Tables 6, 7, and 8, respectively. In the pcDHFR test set, AOS moderately improved the predictive r^2 from 0.438 to 0.461. AOS also slightly reduced the average absolute residual value from 0.58 for conventional CoMFA to 0.56. Using the AOS model, the pIC₅₀ values of 57% of the compounds were predicted with an absolute value of residuals less than 0.5, while for 84% of the compounds the pIC₅₀ values were predicted with this value less than 1.0. The graphs of the actual pIC₅₀ versus the predicted pIC₅₀ values for the training set and test set by the conventional and AOS CoMFA models based on the pcDHFR inhibitory activity are shown in Figure 3A and Figure 3B, respectively. In the tgDHFR test set, AOS moderately improved the predictive r^2 from 0.490 to 0.505. AOS also reduced the average absolute residual value from 0.53 for conventional CoMFA to 0.47. Using the AOS model, the pIC₅₀ values of 67% of the compounds were predicted with an absolute value of residuals less than 0.5, while for 87% of the compounds the pIC₅₀ values were predicted with this value

Table 3. CoMFA Actual and Predicted Activities for pc Training Set Molecules

compd	IC ₅₀ (μM)	pIC ₅₀	conventional CoMFA		AOS CoMFA		CoMSIA	
			calcd	residual	calcd	residual	calcd	residual
1	0.086	7.0655	7.225	0.1595	7.242	0.1765	6.858	-0.2075
2	0.0132	7.8794	7.706	-0.1734	7.621	-0.2584	7.756	-0.1234
4	0.32	6.4949	7.304	0.8091	7.374	0.8791	6.667	0.1721
8	0.52	6.2840	6.246	-0.0380	6.135	-0.1490	6.012	-0.2720
10	0.046	7.3372	6.968	-0.3692	7.26	-0.0772	6.963	-0.3742
11	0.216	6.6655	6.583	-0.0825	7.016	0.3505	6.884	0.2185
12	0.0767	7.1152	6.809	-0.3062	7.025	-0.0902	6.982	-0.1332
13	3.1	5.5086	5.946	0.4374	5.874	0.3654	7.252	1.7434
14	0.51	6.2924	6.786	0.4936	6.572	0.2796	7.198	0.9056
15	0.32	6.4949	7.211	0.7161	6.902	0.4071	7.395	0.9001
20	0.041	7.3872	6.925	-0.4622	7.385	-0.0022	6.732	-0.6552
22	0.0134	7.8729	7.833	-0.0399	7.985	0.1121	7.774	-0.0989
24	1.5	5.8239	6.115	0.2911	5.916	0.0921	6.057	0.2331
26	0.19	6.7212	6.771	0.0498	6.426	-0.2952	7.022	0.3008
29	5	5.3010	5.586	0.2850	5.649	0.3480	6.346	1.0450
31	0.29	6.5376	6.152	-0.3856	6.003	-0.5346	6.215	-0.3226
32	61.7	4.2097	4.89	0.6803	4.696	0.4863	4.414	0.2043
33	7.7	5.1135	4.517	-0.5965	4.96	-0.1535	5.253	0.1395
35	279	3.5544	4.873	1.3186	4.523	0.9686	3.886	0.3316
36	45.7	4.3401	4.15	-0.1901	3.844	-0.4961	3.928	-0.4121
40	19	4.7212	5.005	0.2838	4.712	-0.0092	5.224	0.5028
41	13.5	4.8697	5.127	0.2573	4.918	0.0483	5.361	0.4913
43	7.7	5.1135	4.7	-0.4135	4.9	-0.2135	5.111	-0.0025
47	284	3.5467	4.087	0.5403	4.157	0.6103	4.496	0.9493
51	2	5.6990	5.863	0.1640	6.09	0.3910	5.736	0.0370
52	1.7	5.7696	5.924	0.1544	5.795	0.0254	6.287	0.5174
53	2.7	5.5686	5.698	0.1294	5.83	0.2614	6.618	1.0494
54	0.53	6.2757	6.087	-0.1887	6.081	-0.1947	6.185	-0.0907
57	1.7	5.7696	5.858	0.0884	6.201	0.4314	5.881	0.1114
58	0.66	6.1805	6.251	0.0705	6.301	0.1205	6.048	-0.1325
60	0.85	6.0706	5.974	-0.0966	6.09	0.0194	5.888	-0.1826
61	0.21	6.6778	6.405	-0.2728	6.68	0.0022	6.798	0.1202
63	2	5.6990	6.137	0.4380	6.216	0.5170	6.004	0.3050
64	0.091	7.0410	6.448	-0.5930	6.722	-0.3190	6.926	-0.1150
65	0.16	6.7959	6.754	-0.0419	6.999	0.2031	6.847	0.0511
68	0.04	7.3979	6.885	-0.5129	7.018	-0.3799	6.57	-0.8279
70	0.038	7.4202	7.211	-0.2092	6.952	-0.4682	7.076	-0.3442
73	0.5	6.3010	6.384	0.0830	6.283	-0.0180	6.584	0.2830
75	0.15	6.8239	6.438	-0.3859	6.504	-0.3199	6.547	-0.2769
77	0.17	6.7696	6.331	-0.4386	6.186	-0.5836	5.962	-0.8076
81	0.47	6.3279	6.535	0.2071	6.382	0.0541	6.387	0.0591
83	0.23	6.6383	6.245	-0.3933	6.371	-0.2673	6.412	-0.2263
85	28.3	4.5482	4.378	-0.1702	4.116	-0.4322	4.175	-0.3732
88	11.1	4.9547	4.862	-0.0927	4.502	-0.4527	4.53	-0.4247
89	10.6	4.9747	4.86	-0.1147	4.61	-0.3647	4.651	-0.3237
92	4.6	5.3372	5.73	0.3928	5.634	0.2968	5.497	0.1598
93	2.2	5.6576	5.316	-0.3416	5.337	-0.3206	5.385	-0.2726
94	8.7	5.0605	5.741	0.6805	5.292	0.2315	5.225	0.1645
99	0.052	7.2840	7.383	0.0990	7.366	0.0820	6.896	-0.3880
101	5.4	5.2676	5.052	-0.2156	5.065	-0.2026	5.264	-0.0036
102	0.017	7.7696	7.333	-0.4366	7.228	-0.5416	6.891	-0.8786
104	0.1	7.0000	6.951	-0.0490	7.009	0.0090	6.556	-0.4440
105	0.023	7.6383	6.744	-0.8943	6.754	-0.8843	6.94	-0.6983
106	0.0554	7.2565	7.339	0.0825	7.337	0.0805	6.684	-0.5725
108	0.0954	7.0205	6.731	-0.2895	6.77	-0.2505	6.491	-0.5295
112	0.03	7.5229	7.088	-0.4349	7.29	-0.2329	7.257	-0.2659
113	0.08	7.0969	6.924	-0.1729	7.136	0.0391	6.28	-0.8169
115	0.037	7.4318	7.762	0.3302	7.743	0.3112	7.699	0.2672
117	0.29	6.5376	6.619	0.0814	6.19	-0.3476	6.296	-0.2416
119	0.41	6.3872	6.569	0.1818	6.47	0.0828	6.325	-0.0622
123	1.8	5.7447	5.783	0.0383	5.849	0.1043	5.538	-0.2067
124	0.62	6.2076	6.753	0.5454	6.443	0.2354	6.577	0.3694
125	0.064	7.1938	7.117	-0.0768	7.079	-0.1148	6.371	-0.8228
126	4.28	5.3686	5.425	0.0564	5.437	0.0684	4.969	-0.3996
128	4.6	5.3372	5.664	0.3268	5.445	0.1078	5.715	0.3778
130	0.517	6.2865	6.415	0.1285	6.438	0.1515	6.419	0.1325
132	0.095	7.0223	6.225	-0.7973	6.408	-0.6143	6.104	-0.9183
134	0.246	6.6091	6.403	-0.2061	6.497	-0.1121	7.038	0.4289
138	0.319	6.4962	6.618	0.1218	6.31	-0.1862	6.532	0.0358
140	1.57	5.8041	6.044	0.2399	6.037	0.2329	6.765	0.9609
141	0.41	6.3872	6.085	-0.3022	6.277	-0.1102	6.31	-0.0772
144	3.1	5.5086	5.76	0.2514	5.927	0.4184	5.639	0.1304
146	0.171	6.7670	6.945	0.1780	7.117	0.3500	6.825	0.0580
147	0.114	6.9431	6.31	-0.6331	6.186	-0.7571	6.97	0.0269
149	4.6	5.3372	5.814	0.4768	5.867	0.5298	6.061	0.7238

Table 3 (Continued)

compd	IC ₅₀ (μM)	pIC ₅₀	conventional CoMFA		AOS CoMFA		CoMSIA	
			calcd	residual	calcd	residual	calcd	residual
151	0.7	6.1549	5.088	-1.0669	5.672	-0.4829	5.755	-0.3999
153	3.2	5.4949	5.501	0.0061	5.982	0.4871	5.665	0.1701
154	8.7	5.0605	4.834	-0.2265	4.698	-0.3625	4.936	-0.1245
156	40.4	4.3936	5.567	1.1734	5.039	0.6454	5.403	1.0094
157	16.1	4.7932	4.825	0.0318	4.769	-0.0242	5.02	0.2268
163	0.084	7.0757	7.182	0.1063	7.024	-0.0517	6.696	-0.3797
166	14.1	4.8508	5.028	0.1772	5.233	0.3822	5.186	0.3352
167	0.061	7.2147	7.051	-0.1637	7.042	-0.1727	6.565	-0.6497
168	3.8	5.4202	5.946	0.5258	5.416	-0.0042	5.275	-0.1452
170	24.3	4.6144	4.479	-0.1354	4.832	0.2176	4.847	0.2326
172	4.8	5.3188	4.556	-0.7628	4.983	-0.3358	5.219	-0.0998
173	0.076	7.1192	7.625	0.5058	7.458	0.3388	6.681	-0.4382
174	5.7	5.2441	4.869	-0.3751	5.078	-0.1661	5.205	-0.0391
178	9.2	5.0362	5.017	-0.0192	4.939	-0.0972	5.632	0.5958
179	1.94	5.7122	5.485	-0.2272	5.608	-0.1042	5.238	-0.4742

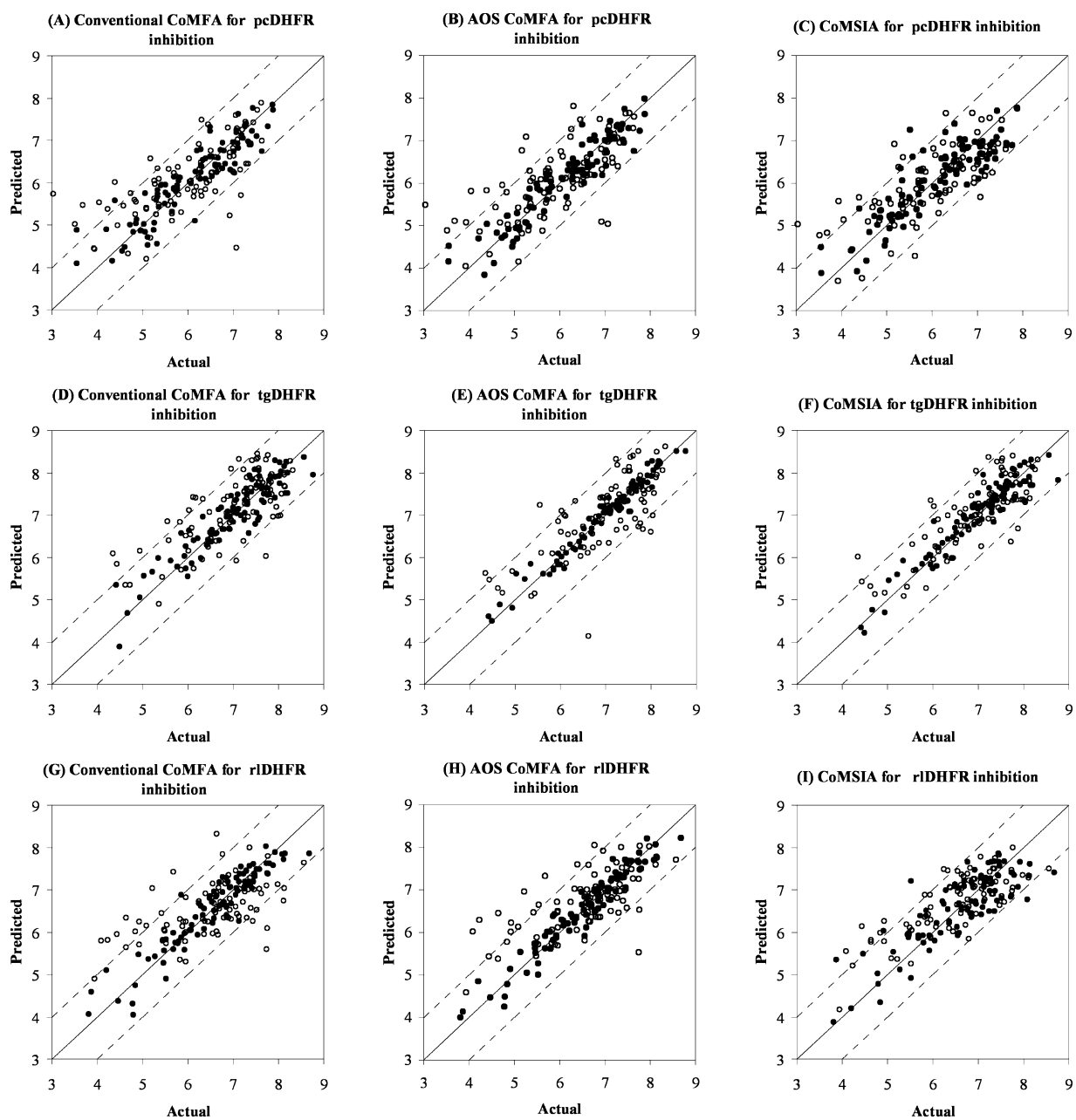


Figure 3. CoMFA and CoMSIA predictions for the training (●) and test (○) sets for DHFR inhibitory activities. The solid line is the regression line for the training set predictions whereas the dotted lines indicate the ± 1.0 log point error margins.

Table 4. CoMFA Actual and Predicted Activities for tg Training Set Molecules

compd	IC ₅₀ (μM)	pIC ₅₀	conventional CoMFA		AOS CoMFA		CoMSIA	
			calcd	residual	calcd	residual	calcd	residual
2	0.00058	9.2366	8.84	-0.3966	9.438	0.2014	8.836	-0.4006
5	0.083	7.0809	7.027	-0.0539	7.168	0.0871	6.892	-0.1889
6	0.027	7.5686	8.06	0.4914	7.641	0.0724	7.492	-0.0766
7	0.012	7.9208	8.291	0.3702	8.204	0.2832	8.16	0.2392
10	0.016	7.7959	7.826	0.0301	7.714	-0.0819	8.074	0.2781
11	0.0301	7.5214	7.696	0.1746	7.541	0.0196	7.928	0.4066
13	0.1	7.0000	7.164	0.1640	7.09	0.0900	7.507	0.5070
16	0.0088	8.0555	8.022	-0.0335	8.057	0.0015	7.787	-0.2685
17	0.0565	7.2480	6.876	-0.3720	7.202	-0.0460	7.638	0.3900
20	0.023	7.6383	7.345	-0.2933	7.617	-0.0213	7.613	-0.0253
22	0.0067	8.1739	8.251	0.0771	8.279	0.1051	8.297	0.1231
23	0.0027	8.5686	8.358	-0.2106	8.506	-0.0626	8.413	-0.1556
24	0.3	6.5229	6.359	-0.1639	6.668	0.1451	6.584	0.0611
26	0.049	7.3098	7.247	-0.0628	7.115	-0.1948	7.368	0.0582
27	1.4	5.8539	6.562	0.7081	5.702	-0.1519	5.978	0.1241
30	0.2	6.6990	6.402	-0.2970	6.667	-0.0320	6.975	0.2760
34	1.1	5.9586	5.732	-0.2266	5.823	-0.1356	5.827	-0.1316
35	6	5.2218	5.654	0.4322	5.477	0.2552	5.584	0.3622
36	1.7	5.7696	5.772	0.0024	5.589	-0.1806	5.837	0.0674
38	1.1	5.9586	6.254	0.2954	6.083	0.1244	6.038	0.0794
42	38	4.4202	5.343	0.9228	4.597	0.1768	4.34	-0.0802
44	32.4	4.4895	3.887	-0.6025	4.489	-0.0005	4.215	-0.2745
46	11.6	4.9355	5.045	0.1095	4.802	-0.1335	4.686	-0.2495
47	21.5	4.6676	4.674	0.0064	4.871	0.2034	4.759	0.0914
50	0.09	7.0458	7.096	0.0502	7.086	0.0402	7.194	0.1482
52	0.1	7.0000	6.833	-0.1670	7.055	0.0550	7.147	0.1470
53	0.12	6.9208	6.947	0.0262	7.179	0.2582	7.244	0.3232
56	0.016	7.7959	7.482	-0.3139	7.699	-0.0969	7.375	-0.4209
57	0.085	7.0706	7.359	0.2884	7.401	0.3304	7.18	0.1094
59	0.028	7.5528	6.869	-0.6838	7.074	-0.4788	7.12	-0.4328
60	0.054	7.2676	7.344	0.0764	7.148	-0.1196	7.2	-0.0676
64	0.0098	8.0088	7.919	-0.0898	7.919	-0.0898	7.786	-0.2228
66	0.015	7.8239	7.907	0.0831	7.81	-0.0139	7.93	0.1061
68	0.018	7.7447	7.633	-0.1117	7.841	0.0963	7.7	-0.0447
72	0.038	7.4202	7.837	0.4168	7.309	-0.1112	7.345	-0.0752
75	0.025	7.6021	7.653	0.0509	7.784	0.1819	7.713	0.1109
78	0.044	7.3565	7.926	0.5695	7.404	0.0475	7.471	0.1145
79	0.13	6.8861	7.073	0.1869	7.205	0.3189	7.177	0.2909
80	0.05	7.3010	7.493	0.1920	7.284	-0.0170	7.047	-0.2540
82	0.048	7.3188	7.241	-0.0778	7.199	-0.1198	7.198	-0.1208
83	0.026	7.5850	6.937	-0.6480	7.627	0.0420	7.373	-0.2120
84	0.14	6.8539	6.946	0.0921	6.965	0.1111	6.958	0.1041
85	1	6.0000	5.542	-0.4580	5.828	-0.1720	5.732	-0.2680
89	0.81	6.0915	5.847	-0.2445	5.723	-0.3685	5.784	-0.3075
90	9.2	5.0362	5.558	0.5218	5.608	0.5718	5.445	0.4088
94	0.32	6.4949	6.58	0.0851	6.472	-0.0229	6.693	0.1981
95	0.17	6.7696	6.658	-0.1116	6.849	0.0794	6.725	-0.0446
97	0.0093	8.0315	8.24	0.2085	8.275	0.2435	8.244	0.2125
100	0.099	7.0044	7.099	0.0946	7.047	0.0426	6.839	-0.1654
101	0.124	6.9066	6.679	-0.2276	6.804	-0.1026	6.767	-0.1396
102	0.021	7.6778	7.489	-0.1888	7.553	-0.1248	7.719	0.0412
104	0.039	7.4089	7.544	0.1351	7.44	0.0311	7.743	0.3341
108	0.012	7.9208	7.894	-0.0268	7.932	0.0112	7.716	-0.2048
109	0.023	7.6383	7.667	0.0287	7.629	-0.0093	7.783	0.1447
110	0.0095	8.0223	7.746	-0.2763	7.649	-0.3733	7.324	-0.6983
111	0.0073	8.1367	8.142	0.0053	8.138	0.0013	7.893	-0.2437
112	0.0063	8.2007	8	-0.2007	8.21	0.0093	8.134	-0.0667
113	0.0017	8.7696	7.945	-0.8246	8.511	-0.2586	7.822	-0.9476
119	0.049	7.3098	7.465	0.1552	7.235	-0.0748	7.145	-0.1648
120	0.077	7.1135	7.142	0.0285	7.09	-0.0235	7.952	0.8385
122	0.033	7.4815	8.064	0.5825	7.335	-0.1465	7.649	0.1675
123	0.6	6.2218	6.449	0.2272	6.301	0.0792	6.328	0.1062
125	0.068	7.1675	6.983	-0.1845	7.233	0.0655	7.27	0.1025
127	0.052	7.2840	7.617	0.3330	7.288	0.0040	7.29	0.0060
129	0.29	6.5376	6.639	0.1014	6.452	-0.0856	6.835	0.2974
131	0.023	7.6383	7.615	-0.0233	7.613	-0.0253	7.718	0.0797
132	0.007	8.1549	7.514	-0.6409	8.185	0.0301	7.696	-0.4589
133	0.11	6.9586	7.454	0.4954	7.051	0.0924	7.163	0.2044
134	0.021	7.6778	7.293	-0.3848	7.702	0.0242	7.766	0.0882
135	0.054	7.2676	7.048	-0.2196	7.322	0.0544	7.238	-0.0296
136	0.03	7.5229	7.048	-0.4749	7.085	-0.4379	7.438	-0.0849
139	0.181	6.7423	7.164	0.4217	6.818	0.0757	6.896	0.1537
142	0.078	7.1079	7.477	0.3691	7.026	-0.0819	7.223	0.1151
147	0.017	7.7696	7.465	-0.3046	7.812	0.0424	7.702	-0.0676
148	0.012	7.9208	7.401	-0.5198	7.756	-0.1648	7.724	-0.1968

Table 4 (Continued)

compd	IC ₅₀ (μM)	pIC ₅₀	conventional CoMFA		AOS CoMFA		CoMSIA	
			calcd	residual	calcd	residual	calcd	residual
151	0.045	7.3468	6.572	-0.7748	7.15	-0.1968	6.827	-0.5198
153	0.21	6.6778	7.119	0.4412	6.588	-0.0898	6.987	0.3092
154	0.46	6.3372	6.952	0.6148	6.175	-0.1622	6.433	0.0958
157	0.73	6.1367	6.394	0.2573	6.094	-0.0427	6.227	0.0903
158	2.4	5.6198	5.92	0.3002	5.601	-0.0188	5.696	0.0762
161	0.032	7.4949	6.783	-0.7119	7.329	-0.1659	7.103	-0.3919
162	0.92	6.0362	6.622	0.5858	6.006	-0.0302	6.85	0.8138
163	0.0063	8.2007	7.509	-0.6917	8.234	0.0333	7.694	-0.5067
164	0.35	6.4559	6.404	-0.0519	6.239	-0.2169	6.472	0.0161
169	0.23	6.6383	6.561	-0.0773	6.9	0.2617	6.533	-0.1053
171	0.026	7.5850	7.922	0.3370	7.726	0.1410	7.495	-0.0900
174	1.2	5.9208	6.019	0.0982	5.903	-0.0178	6.053	0.1322
176	0.38	6.4202	6.285	-0.1352	6.369	-0.0512	5.979	-0.4412
177	0.52	6.2840	5.971	-0.3130	6.212	-0.0720	6.022	-0.2620
179	4.45	5.3516	5.983	0.6314	5.833	0.4814	5.908	0.5564
134	0.021	7.6778	7.293	-0.3848	7.702	0.0242	7.766	0.0882
135	0.054	7.2676	7.048	-0.2196	7.322	0.0544	7.238	-0.0296
136	0.03	7.5229	7.048	-0.4749	7.085	-0.4379	7.438	-0.0849
139	0.181	6.7423	7.164	0.4217	6.818	0.0757	6.896	0.1537
142	0.078	7.1079	7.477	0.3691	7.026	-0.0819	7.223	0.1151
147	0.017	7.7696	7.465	-0.3046	7.812	0.0424	7.702	-0.0676
148	0.012	7.9208	7.401	-0.5198	7.756	-0.1648	7.724	-0.1968
151	0.045	7.3468	6.572	-0.7748	7.15	-0.1968	6.827	-0.5198
153	0.21	6.6778	7.119	0.4412	6.588	-0.0898	6.987	0.3092
154	0.46	6.3372	6.952	0.6148	6.175	-0.1622	6.433	0.0958
157	0.73	6.1367	6.394	0.2573	6.094	-0.0427	6.227	0.0903
158	2.4	5.6198	5.92	0.3002	5.601	-0.0188	5.696	0.0762
161	0.032	7.4949	6.783	-0.7119	7.329	-0.1659	7.103	-0.3919
162	0.92	6.0362	6.622	0.5858	6.006	-0.0302	6.85	0.8138
163	0.0063	8.2007	7.509	-0.6917	8.234	0.0333	7.694	-0.5067
164	0.35	6.4559	6.404	-0.0519	6.239	-0.2169	6.472	0.0161
169	0.23	6.6383	6.561	-0.0773	6.9	0.2617	6.533	-0.1053
171	0.026	7.5850	7.922	0.3370	7.726	0.1410	7.495	-0.0900
174	1.2	5.9208	6.019	0.0982	5.903	-0.0178	6.053	0.1322
176	0.38	6.4202	6.285	-0.1352	6.369	-0.0512	5.979	-0.4412
177	0.52	6.2840	5.971	-0.3130	6.212	-0.0720	6.022	-0.2620
179	4.45	5.3516	5.983	0.6314	5.833	0.4814	5.908	0.5564

less than 1.0. The graphs of the actual pIC₅₀ versus the predicted pIC₅₀ values for the training set and test set by the conventional and AOS CoMFA models based on the tgDHFR inhibitory activity are shown in Figure 3D and Figure 3E, respectively. In the rat liver DHFR test set, AOS significantly improved the predictive r^2 from 0.337 to 0.421. AOS also reduced the average absolute residual value from 0.71 for conventional CoMFA to 0.57. Using the AOS model, the pIC₅₀ values of 55% of the compounds were predicted with an absolute value of residuals less than 0.5, while for 81% of the compounds the pIC₅₀ values were predicted with this value less than 1.0. The graphs of the actual pIC₅₀ versus the predicted pIC₅₀ values for the training set and test set by the conventional and AOS CoMFA models based on the rat liver DHFR inhibitory activity are shown in Figure 3G and Figure 3H, respectively. Given that the actual pIC₅₀ values of the compounds within each test set against the appropriate enzyme fluctuate within a range of at least 3 logarithm units, the fact that all three AOS CoMFA models predicted the activity of more than 80% of the corresponding test set compounds within 1 logarithm unit from the experimentally determined value further verified the predictability of the models.

5.2. CoMSIA Analysis. Three CoMSIA models, one for each enzyme, were generated from the same training sets used in CoMFA analysis. The key statistical parameters associated with these models are shown in Table 2 along with the data of the CoMFA models. As in the case of CoMFA models, the predicted pIC₅₀ values for the pcDHFR, tgDHFR, and rLDHFR training set compounds and the residual values are given in Tables 3, 4, and 5, respectively. The graphs of the actual pIC₅₀ versus the predicted pIC₅₀ values for the training set and test set by the CoMSIA models based on the pcDHFR, tgDHFR, and rLDHFR inhibitory activity are shown in Figure 3C, Figure

3F, and Figure 3I, respectively. The cross-validated r^2 values (q^2) for pcDHFR, tgDHFR, and rat liver DHFR training sets are 0.542 (ONC = 3), 0.461 (ONC = 7), and 0.475 (ONC = 2), respectively. The average absolute residual value for each model is 0.38, 0.22, and 0.18, respectively. As in the case of CoMFA analyses, we attempted to predict the inhibitory activity against pcDHFR, tgDHFR, and rLDHFR for the 89 compounds in each corresponding test set, respectively. The predictive r^2 values were obtained and are shown in Table 2. The predicted pIC₅₀ values for pcDHFR, tgDHFR, and rLDHFR test set compounds as well as the residual values are given in Table 6, 7, and 8, respectively. The average absolute residual value for each model is 0.55, 0.41, and 0.53, respectively. The pIC₅₀ values of 48% of the pcDHFR test set compounds were predicted with an absolute value of residuals less than 0.5, while for 85% of the compounds the pIC₅₀ values were predicted with this value less than 1.0. The pIC₅₀ values of 72% of the tgDHFR test set compounds were predicted with an absolute value of residuals less than 0.5, while for 89% of the compounds the pIC₅₀ values were predicted with this value less than 1.0. The pIC₅₀ values of 58% of the rat liver DHFR test set compounds were predicted with an absolute value of residuals less than 0.5, while for 85% of the compounds the pIC₅₀ values were predicted with this value less than 1.0. Although the q^2 values in the training sets associated with these CoMSIA models are generally inferior to those of their AOS CoMFA counterparts, their predictive r^2 values in the test sets are unanimously higher. Thus, the CoMSIA models seem to have even better predictive power than the AOS CoMFA model.

5.3. CoMFA and CoMSIA Contour Maps. Because AOS CoMFA models gave the highest cross-validated r^2 and CoMSIA models gave the highest predictive r^2 , we decided to use these models for further evaluation.

Table 5. CoMFA Actual and Predicted Activities for rl Training Set Molecules

compd	IC ₅₀ (μM)	pIC ₅₀	conventional CoMFA		AOS CoMFA		CoMSIA	
			calcd	residual	calcd	residual	calcd	residual
1	0.0021	8.6778	8.376	-0.3018	8.623	-0.0548	8.062	-0.6158
4	0.053	7.2757	7.211	-0.0647	7.069	-0.2067	7.341	0.0653
5	0.14	6.8539	6.852	-0.0019	6.822	-0.0319	6.887	0.0331
7	0.033	7.4815	7.486	0.0045	7.545	0.0635	7.484	0.0025
13	3	5.5229	5.571	0.0481	5.674	0.1511	5.629	0.1061
14	0.33	6.4815	6.401	-0.0805	6.448	-0.0335	6.335	-0.1465
16	0.0076	8.1192	8.335	0.2158	8.132	0.0128	8.035	-0.0842
18	0.0425	7.3716	7.464	0.0924	7.543	0.1714	7.41	0.0384
19	0.17	6.7696	6.787	0.0174	6.836	0.0664	7.48	0.7104
20	0.054	7.2676	7.421	0.1534	7.43	0.1624	7.501	0.2334
21	0.0118	7.9281	8.047	0.1189	7.943	0.0149	7.877	-0.0511
22	0.0175	7.7570	7.822	0.0650	7.754	-0.0030	7.679	-0.0780
24	1.9	5.7212	5.72	-0.0012	5.779	0.0578	5.975	0.2538
30	0.61	6.2147	6.223	0.0083	6.207	-0.0077	6.204	-0.0107
31	0.26	6.5850	6.659	0.0740	6.47	-0.1150	6.369	-0.2160
33	2.1	5.6778	5.721	0.0432	5.71	0.0322	5.761	0.0832
34	7.4	5.1308	5.172	0.0412	5.156	0.0252	5.252	0.1212
35	63	4.2007	4.851	0.6503	4.464	0.2633	4.353	0.1523
36	156	3.8069	3.79	-0.0169	3.66	-0.1469	3.877	0.0701
37	14.4	4.8416	4.683	-0.1586	4.623	-0.2186	4.926	0.0844
43	137	3.8633	3.871	0.0077	3.924	0.0607	3.658	-0.2053
44	16.2	4.7905	4.939	0.1485	5.052	0.2615	4.709	-0.0815
46	12.3	4.9101	4.786	-0.1241	4.863	-0.0471	5.116	0.2059
47	34.3	4.4647	4.627	0.1623	4.708	0.2433	5.098	0.6333
51	0.14	6.8539	6.82	-0.0339	6.896	0.0421	6.986	0.1321
52	0.2	6.6990	6.718	0.0190	6.553	-0.1460	6.689	-0.0100
55	0.2	6.6990	6.835	0.1360	6.657	-0.0420	6.869	0.1700
56	0.018	7.7447	7.718	-0.0267	7.771	0.0263	7.76	0.0153
57	0.26	6.5850	6.863	0.2780	6.92	0.3350	6.855	0.2700
58	0.044	7.3565	7.298	-0.0585	7.23	-0.1265	7.152	-0.2045
60	0.073	7.1367	7.16	0.0233	7.093	-0.0437	7.088	-0.0487
65	0.016	7.7959	7.97	0.1741	7.909	0.1131	7.519	-0.2769
66	0.035	7.4559	7.301	-0.1549	7.242	-0.2139	7.097	-0.3589
67	0.0072	8.1427	8.17	0.0273	8.163	0.0203	8.025	-0.1177
73	0.058	7.2366	7.436	0.1994	7.303	0.0664	7.25	0.0134
76	0.12	6.9208	6.886	-0.0348	7.077	0.1562	7.294	0.3732
77	0.048	7.3188	7.225	-0.0938	7.195	-0.1238	7.324	0.0052
78	0.052	7.2840	7.429	0.1450	7.521	0.2370	7.333	0.0490
79	0.52	6.2840	6.646	0.3620	6.577	0.2930	6.7	0.4160
80	0.088	7.0555	6.951	-0.1045	7.073	0.0175	6.884	-0.1715
82	0.086	7.0655	6.962	-0.1035	7.051	-0.0145	6.798	-0.2675
84	0.32	6.4949	6.407	-0.0879	6.505	0.0101	6.436	-0.0589
85	3	5.5229	5.329	-0.1939	5.266	-0.2569	5.028	-0.4949
87	5.3	5.2757	5.312	0.0363	5.176	-0.0997	5.142	-0.1337
88	16.7	4.7773	4.67	-0.1073	4.748	-0.0293	4.506	-0.2713
91	0.9	6.0458	6.186	0.1402	6.272	0.2262	6.057	0.0112
94	0.66	6.1805	6.137	-0.0435	6.25	0.0695	6.4	0.2195
95	1.2	5.9208	5.735	-0.1858	6.077	0.1562	6.149	0.2282
97	0.0082	8.0862	8.034	-0.0522	8.015	-0.0712	8.014	-0.0722
99	0.019	7.7212	7.697	-0.0242	7.735	0.0138	7.746	0.0248
101	1.6	5.7959	5.474	-0.3219	5.762	-0.0339	5.932	0.1361
104	0.043	7.3665	7.335	-0.0315	7.416	0.0495	7.54	0.1735
106	0.051	7.2924	7.285	-0.0074	7.198	-0.0944	7.022	-0.2704
109	0.169	6.7721	6.773	0.0009	6.882	0.1099	6.796	0.0239
111	0.013	7.8861	7.458	-0.4281	7.798	-0.0881	7.621	-0.2651
114	0.026	7.5850	7.623	0.0380	7.507	-0.0780	7.536	-0.0490
115	0.036	7.4437	7.616	0.1723	7.543	0.0993	7.537	0.0933
116	0.0801	7.0964	7.168	0.0716	7.123	0.0266	7.075	-0.0214
118	0.17	6.7696	6.925	0.1554	6.914	0.1444	6.823	0.0534
119	0.23	6.6383	6.574	-0.0643	6.386	-0.2523	6.547	-0.0913
121	0.13	6.8861	6.853	-0.0331	6.708	-0.1781	7.038	0.1519
123	3.5	5.4559	5.453	-0.0029	5.421	-0.0349	5.591	0.1351
125	0.44	6.3565	6.149	-0.2075	6.351	-0.0055	6.69	0.3335
127	0.086	7.0655	6.991	-0.0745	6.935	-0.1305	6.833	-0.2325
128	0.47	6.3279	6.335	0.0071	6.302	-0.0259	6.223	-0.1049
130	0.139	6.8570	6.892	0.0350	6.937	0.0800	6.996	0.1390
132	0.038	7.4202	7.625	0.2048	7.529	0.1088	7.353	-0.0672
134	0.034	7.4685	7.354	-0.1145	7.487	0.0185	7.452	-0.0165
135	0.29	6.5376	6.585	0.0474	6.579	0.0414	6.382	-0.1556
137	0.109	6.9626	6.881	-0.0816	6.636	-0.3266	7.092	0.1294
138	0.116	6.9355	6.942	0.0065	6.91	-0.0255	6.724	-0.2115
139	0.56	6.2518	6.249	-0.0028	6.325	0.0732	6.396	0.1442
144	1.63	5.7878	5.675	-0.1128	5.709	-0.0788	5.609	-0.1788
146	0.067	7.1739	7.241	0.0671	7.166	-0.0079	7.361	0.1871
147	0.071	7.1487	7.017	-0.1317	7.124	-0.0247	6.859	-0.2897

Table 5 (Continued)

compd	IC ₅₀ (μM)	pIC ₅₀	conventional CoMFA		AOS CoMFA		CoMSIA	
			calcd	residual	calcd	residual	calcd	residual
151	0.075	7.1249	6.517	-0.6079	6.725	-0.3999	6.89	-0.2349
153	1.4	5.8539	6.033	0.1791	5.734	-0.1199	5.874	0.0201
154	0.26	6.5850	6.357	-0.2280	6.505	-0.0800	6.441	-0.1440
157	3.6	5.4437	5.671	0.2273	5.532	0.0883	5.811	0.3673
160	0.82	6.0862	6.138	0.0518	6.216	0.1298	6.074	-0.0122
161	0.14	6.8539	6.647	-0.2069	6.724	-0.1299	6.297	-0.5569
162	1.4	5.8539	6.154	0.3001	5.998	0.1441	6.443	0.5891
163	0.057	7.2441	7.288	0.0439	7.312	0.0679	7.426	0.1819
164	3.3	5.4815	5.285	-0.1965	5.532	0.0505	5.273	-0.2085
169	1.2	5.9208	6.048	0.1272	5.837	-0.0838	5.469	-0.4518
171	0.03	7.5229	7.333	-0.1899	7.356	-0.1669	7.547	0.0241
174	3.4	5.4685	5.413	-0.0555	5.377	-0.0915	5.732	0.2635
176	0.43	6.3665	6.311	-0.0555	6.238	-0.1285	6.363	-0.0035
177	2.1	5.6778	5.913	0.2352	5.776	0.0982	6.093	0.4152
179	0.28	6.5528	6.401	-0.1518	6.474	-0.0788	5.813	-0.7398

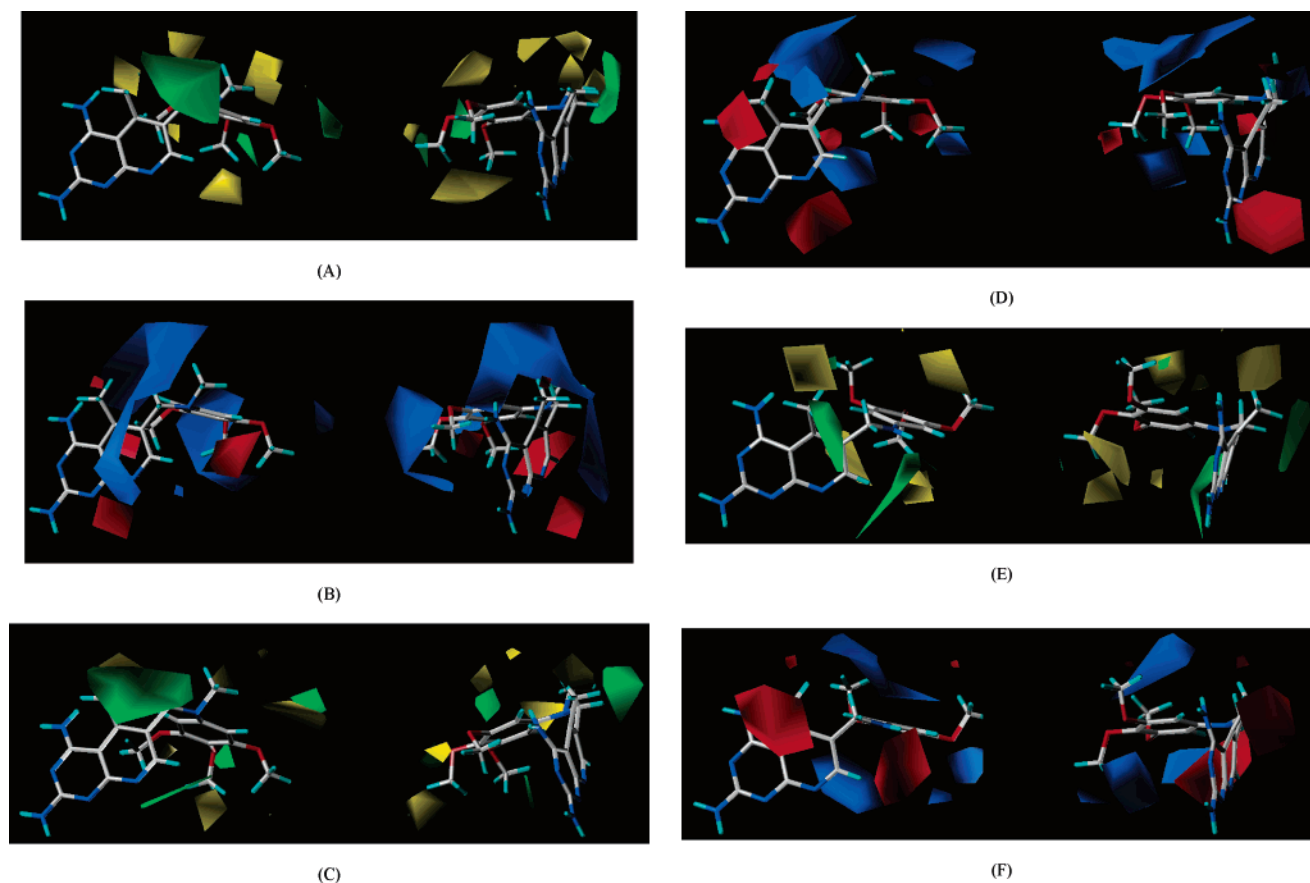


Figure 4. (A) Steric fields generated with the AOS CoMFA model based on pcDHFR inhibitory activity: yellow indicates regions where bulky groups decrease activity, whereas green indicates regions where bulky groups increase activity. (B) Electrostatic fields generated with the AOS CoMFA model based on pcDHFR inhibitory activity: blue indicates regions where more positively charged groups increase activity, whereas red indicates regions where more negatively charged groups increase activity. (C) Steric fields generated with the AOS CoMFA model based on tgDHFR inhibitory activity; the color scheme is the same as in panel A. (D) Electrostatic fields generated with the AOS CoMFA model based on tgDHFR inhibitory activity; the color scheme is the same as in panel B. (E) Steric fields generated with the AOS CoMFA model based on rat liver DHFR inhibitory activity; the color scheme is the same as in panel A. (F) Electrostatic fields generated with the AOS CoMFA model based on rat liver DHFR inhibitory activity; the color scheme is the same as in panel B.

AOS CoMFA analyses were selected to construct the stdev*coefficient contour maps (Figure 4). In the CoMFA steric field, the green (sterically favorable) and yellow (sterically unfavorable) contours represent 80% and 20% level contributions, respectively. Similarly the red (negative charge favorable) and blue (negative charge unfavorable) contours in the CoMFA electrostatic field represent 80% and 20% level contributions, respectively.

CoMSIA analyses were also selected to construct contour maps (Figure 5). Since, for all three CoMSIA models, the combined contribution of electrostatic and hydrophobic descriptors is more than 0.7 or 70%, only these two types of fields were discussed further. In the CoMSIA electrostatic field, the red (negative charge favorable) and blue (negative charge unfavorable) contours represent 80% and 20% level contributions, respectively. Similarly the yellow (hydrophobic favor-

Table 6. CoMFA Actual and Predicted Activities for pc Test Set Molecules

compd	IC ₅₀ (μM)	pIC ₅₀	conventional CoMFA		AOS CoMFA		CoMSIA	
			calcd	residual	calcd	residual	calcd	residual
3	0.55	6.2596	6.324	0.0644	7.2680	1.0084	6.165	-0.0946
5	0.51	6.2924	5.793	-0.4994	6.0280	-0.2644	5.772	-0.5204
6	0.1	7.0000	6.818	-0.1820	6.5450	-0.4550	7.196	0.1960
7	0.063	7.2007	7.241	0.0403	7.1530	-0.0477	6.858	-0.3427
9	0.573	6.2418	6.913	0.6712	7.0870	0.8452	6.271	0.0292
16	0.044	7.3565	6.888	-0.4685	7.2740	-0.0825	6.806	-0.5505
17	0.316	6.5003	6.747	0.2467	6.2460	-0.2543	5.972	-0.5283
18	0.0229	7.6402	6.99	-0.6502	7.5620	-0.0782	6.889	-0.7512
19	0.13	6.8861	7.298	0.4119	7.5050	0.6189	7.648	0.7619
21	0.0535	7.2716	7.441	0.1694	7.0640	-0.2076	7.532	0.2604
23	0.497	6.3036	7.488	1.1844	7.8100	1.5064	7.642	1.3384
25	0.24	6.6198	6.386	-0.2338	6.3720	-0.2478	6.904	0.2842
27	2.6	5.5850	6.32	0.7350	6.0880	0.5030	5.515	-0.0700
28	5.3	5.2757	5.955	0.6793	5.3610	0.0853	5.832	0.5563
30	1.4	5.8539	5.295	-0.5589	5.6400	-0.2139	6.264	0.4101
34	18.5	4.7328	5.74	1.0072	5.9530	1.2202	5.572	0.8392
37	35.3	4.4522	4.977	0.5248	4.3250	-0.1272	3.764	-0.6882
38	307	3.5129	5.016	1.5031	4.8880	1.3751	4.772	1.2591
39	119	3.9245	4.445	0.5205	4.0480	0.1235	3.699	-0.2255
42	41	4.3872	6.011	1.6238	5.8310	1.4438	5.662	1.2748
44	8.1	5.0915	4.201	-0.8905	4.1530	-0.9385	4.341	-0.7505
45	14.8	4.8297	5.593	0.7633	5.7870	0.9573	5.533	0.7033
46	0.65	6.1871	5.898	-0.2891	5.5260	-0.6611	5.574	-0.6131
48	0.41	6.3872	5.838	-0.5492	6.0780	-0.3092	5.837	-0.5502
49	1.6	5.7959	6.121	0.3251	6.5460	0.7501	6.337	0.5411
50	0.9	6.0458	6.022	-0.0238	6.1170	0.0712	5.918	-0.1278
55	2	5.6990	6.22	0.5210	6.2850	0.5860	6.294	0.5950
56	0.25	6.6021	5.79	-0.8121	6.1800	-0.4221	6.447	-0.1551
59	1	6.0000	5.834	-0.1660	5.8670	-0.1330	5.698	-0.3020
62	4.4	5.3565	6.079	0.7225	6.0470	0.6905	6.608	1.2515
66	0.097	7.0132	6.63	-0.3832	6.9980	-0.0152	6.964	-0.0492
67	0.052	7.2840	6.439	-0.8450	6.3960	-0.8880	6.75	-0.5340
69	0.51	6.2924	6.471	0.1786	6.2500	-0.0424	6.618	0.3256
71	0.29	6.5376	6.243	-0.2946	6.4740	-0.0636	6.535	-0.0026
72	0.25	6.6021	6.432	-0.1701	6.3120	-0.2901	6.536	-0.0661
74	1.6	5.7959	5.72	-0.0759	6.1060	0.3101	5.516	-0.2799
76	0.21	6.6778	6.371	-0.3068	6.4110	-0.2668	6.599	-0.0788
78	0.12	6.9208	6.7	-0.2208	6.8010	-0.1198	6.344	-0.5768
79	2	5.6990	5.843	0.1440	5.5400	-0.1590	6.057	0.3580
80	0.73	6.1367	5.662	-0.4747	6.1180	-0.0187	5.725	-0.4117
82	0.38	6.4202	5.988	-0.4322	6.3020	-0.1182	6.402	-0.0182
84	5.5	5.2596	6.038	0.7784	7.0860	1.8264	6.376	1.1164
86	209	3.6799	5.466	1.7861	5.1110	1.4311	4.83	1.1501
87	58.5	4.2328	5.37	1.1372	4.8620	0.6292	4.442	0.2092
90	929	3.0320	5.728	2.6960	5.4890	2.4570	5.033	2.0010
91	6.8	5.1675	4.693	-0.4745	4.8160	-0.3515	5.004	-0.1635
95	4.4	5.3565	5.483	0.1265	5.5150	0.1585	5.403	0.0465
96	4.9	5.3098	5.246	-0.0638	4.8910	-0.4188	5.488	0.1782
97	0.0238	7.6234	7.877	0.2536	7.2910	-0.3324	6.8	-0.8234
98	116	3.9355	4.431	0.4955	5.0790	1.1435	5.574	1.6385
100	0.72	6.1427	5.784	-0.3587	5.4170	-0.7257	5.295	-0.8477
103	0.087	7.0605	7.586	0.5255	6.9720	-0.0885	6.683	-0.3775
107	0.047	7.3279	6.437	-0.8909	6.9520	-0.3759	6.246	-1.0819
109	0.117	6.9318	6.608	-0.3238	6.3240	-0.6078	6.12	-0.8118
110	0.0808	7.0926	7.276	0.1834	7.3320	0.2394	7.496	0.4034
111	0.035	7.4559	7.42	-0.0359	7.6380	0.1821	6.931	-0.5249
114	0.029	7.5376	7.717	0.1794	7.6480	0.1104	7.484	-0.0536
116	0.0689	7.1618	6.298	-0.8638	6.5910	-0.5708	6.164	-0.9978
118	0.25	6.6021	6.592	-0.0101	6.5970	-0.0051	6.387	-0.2151
120	0.57	6.2441	6.116	-0.1281	6.4030	0.1589	6.953	0.7089
121	0.85	6.0706	6.045	-0.0256	6.6270	0.5564	6.657	0.5864
122	0.35	6.4559	7.372	0.9161	7.4910	1.0351	6.908	0.4521
127	2.4	5.6198	5.556	-0.0638	4.8810	-0.7388	4.286	-1.3338
129	2.2	5.6576	5.261	-0.3966	5.1800	-0.4776	4.951	-0.7066
131	0.1	7.0000	6.251	-0.7490	6.7120	-0.2880	6.442	-0.5580
133	6.8	5.1675	6.568	1.4005	6.7670	1.5995	6.916	1.7485
135	4.6	5.3372	6.338	1.0008	6.2910	0.9538	5.58	0.2428
136	0.33	6.4815	6.042	-0.4395	5.9700	-0.5115	6.5	0.0185
137	0.502	6.2993	5.68	-0.6193	5.8830	-0.4163	5.826	-0.4733
139	1.67	5.7773	6.358	0.5807	6.2710	0.4937	6.048	0.2707
142	0.94	6.0269	6.566	0.5391	6.7440	0.7171	6.815	0.7881
143	0.21	6.6778	6.295	-0.3828	6.1970	-0.4808	6.34	-0.3378
145	0.3	6.5229	6.222	-0.3009	6.1410	-0.3819	6.295	-0.2279
148	0.119	6.9245	5.213	-1.7115	5.0930	-1.8315	6.007	-0.9175
150	2.2	5.6576	5.089	-0.5686	5.7710	0.1134	5.861	0.2034

Table 6 (Continued)

compd	IC ₅₀ (μM)	pIC ₅₀	conventional CoMFA		AOS CoMFA		CoMSIA	
			calcd	residual	calcd	residual	calcd	residual
152	0.086	7.0655	4.451	-2.6145	5.0420	-2.0235	5.67	-1.3955
155	90.4	4.0438	5.532	1.4882	5.8130	1.7692	5.138	1.0942
158	25.9	4.5867	5.455	0.8683	5.4330	0.8463	5.098	0.5113
159	8.3	5.0809	5.409	0.3281	5.0730	-0.0079	5.186	0.1051
160	14.6	4.8356	5.252	0.4164	5.2270	0.3914	5.121	0.2854
161	0.068	7.1675	5.697	-1.4705	6.4790	-0.6885	6.175	-0.9925
162	1.8	5.7447	6.145	0.4003	6.3500	0.6053	6.32	0.5753
164	14.1	4.8508	5.546	0.6952	5.0230	0.1722	5.353	0.5022
165	5.5	5.2596	5.625	0.3654	5.6680	0.4084	5.251	-0.0086
169	20.7	4.6840	4.317	-0.3670	5.0730	0.3890	5.43	0.7460
171	0.079	7.1024	7.017	-0.0854	7.2010	0.0986	6.621	-0.4814
175	3.9	5.4089	5.93	0.5211	6.1180	0.7091	5.553	0.1441
176	8.2	5.0862	5.37	0.2838	5.4230	0.3368	5.515	0.4288
177	2.7	5.5686	5.464	-0.1046	5.2140	-0.3546	5.067	-0.5016

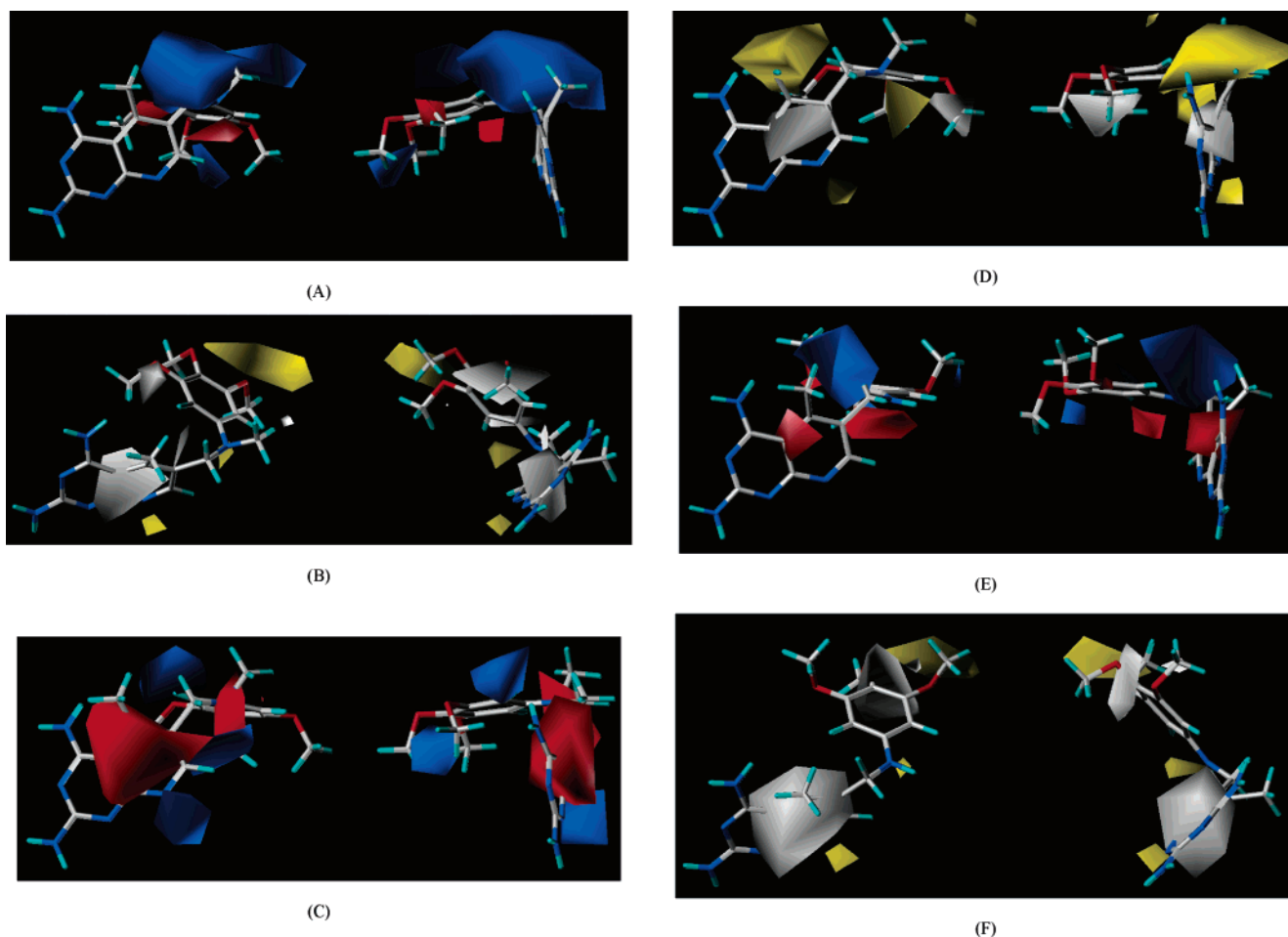


Figure 5. (A) Electrostatic fields generated with the CoMSIA model based on pcDHFR inhibitory activity: blue indicates regions where more positively charged groups increase activity, whereas red indicates regions where more negatively charged groups increase activity. (B) Hydrophobic fields generated with the CoMSIA model based on tgDHFR inhibitory activity: yellow indicates regions where hydrophobic groups decrease activity, whereas white indicates regions where hydrophilic groups increase activity. (C) Electrostatic fields generated with the CoMSIA model based on tgDHFR inhibitory activity; the color scheme is the same as in panel A. (D) Hydrophobic fields generated with the CoMSIA model based on tgDHFR inhibitory activity; the color scheme is the same as in panel B. (E) Electrostatic fields generated with the CoMSIA model based on rat liver DHFR inhibitory activity; the color scheme is the same as in panel A. (F) Hydrophobic fields generated with the CoMSIA model based on rat liver DHFR inhibitory activity; the color scheme is the same as in panel B.

able) and white (hydrophobic unfavorable) contours represents 80% and 20% level contributions, respectively, in the CoMSIA hydrophobic field.

The pcDHFR inhibitory activity CoMFA steric contour map is depicted in Figure 4A. The 5-methyl group falls into a sterically unfavorable yellow region, suggesting that there is a sterically unfavorable region relating to the accessibility of the compounds to the pcDHFR side pocket. Many DHFR

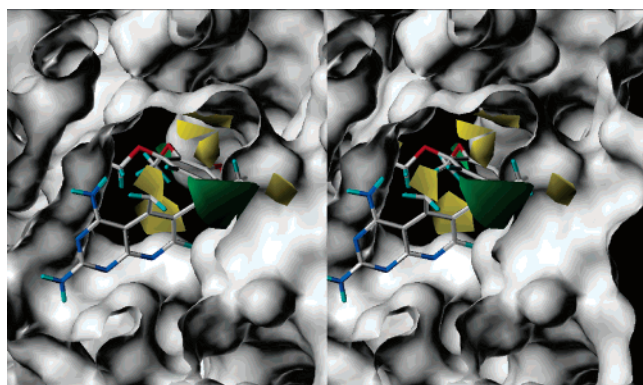
inhibitors with a 6-6 ring system have a 5-methyl group to increase activity. Removing the methyl group will result in a decrease in predicted activity, while replacing the methyl group with a propyl or even bulkier group will also result in a decrease in predicted activity. When replacing the methyl group with an ethyl, the predicted activity goes slightly higher. Thus the best substituent would appear to be a methyl or ethyl group. The 9-substituents (or the 8-position in the case of a

Table 7. CoMFA Actual and Predicted Activities for tg Test Set Molecules

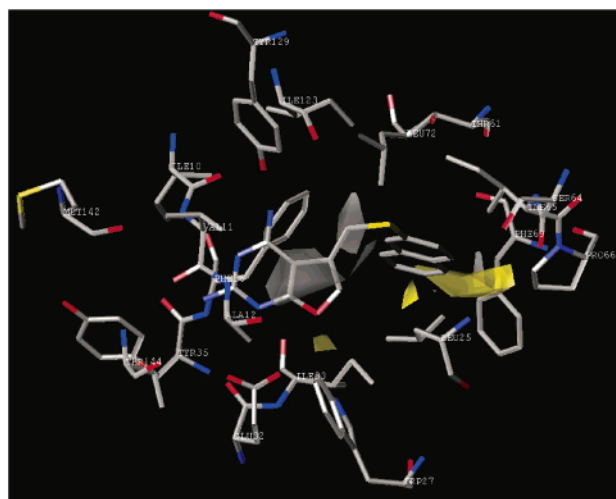
compd	IC ₅₀ (μ M)	pIC ₅₀	conventional CoMFA		AOS CoMFA		CoMSIA	
			calcd	residual	calcd	residual	calcd	residual
1	0.0074	8.1308	7.83	-0.3008	7.75	-0.3808	7.927	-0.2038
3	0.013	7.8861	7.142	-0.7441	7.101	-0.7851	7.052	-0.8341
4	0.028	7.5528	7.707	0.1542	7.736	0.1832	8.025	0.4722
8	0.094	7.0269	6.568	-0.4589	6.526	-0.5009	6.584	-0.4429
9	0.0145	7.8386	7.16	-0.6786	7.099	-0.7396	7.202	-0.6366
12	0.017	7.7696	8.976	1.2064	9.235	1.4654	7.808	0.0384
14	0.038	7.4202	7.619	0.1988	7.79	0.3698	7.934	0.5138
15	0.029	7.5376	7.716	0.1784	7.754	0.2164	7.883	0.3454
18	0.0048	8.3188	7.726	-0.5928	7.886	-0.4328	8.301	-0.0178
19	0.058	7.2366	8.323	1.0864	8.425	1.1884	8.524	1.2874
21	0.0077	8.1135	7.447	-0.6665	6.996	-1.1175	7.937	-0.1765
25	0.009	8.0458	7.479	-0.5668	6.968	-1.0778	7.267	-0.7788
28	1.5	5.8239	6.667	0.8431	6.219	0.3951	6.422	0.5981
29	0.2	6.6990	6.366	-0.3330	6.78	0.0810	6.691	-0.0080
31	0.25	6.6021	6.409	-0.1931	6.291	-0.3111	6.398	-0.2041
32	0.47	6.3279	7.2	0.8721	6.537	0.2091	7.136	0.8081
33	1.1	5.9586	6.807	0.8484	6.672	0.7134	7.467	1.5084
37	1.4	5.8539	5.613	-0.2409	5.765	-0.0889	5.738	-0.1159
39	4.3	5.3665	4.965	-0.4015	5.068	-0.2985	5.229	-0.1375
40	19	4.7212	5.255	0.5338	5.243	0.5218	5.37	0.6488
41	37	4.4318	5.583	1.1512	5.529	1.0972	5.487	1.0552
43	45.4	4.3429	5.839	1.4961	5.699	1.3561	6.424	2.0811
45	23.6	4.6271	5.197	0.5699	5.434	0.8069	4.88	0.2529
48	0.057	7.2441	7.225	-0.0191	6.87	-0.3741	7.174	-0.0701
49	0.16	6.7959	7.132	0.3361	6.331	-0.4649	6.408	-0.3879
51	0.13	6.8861	7.09	0.2039	6.982	0.0959	7.085	0.1989
54	0.11	6.9586	6.862	-0.0966	7.053	0.0944	6.888	-0.0706
55	0.04	7.3979	7.269	-0.1289	7.281	-0.1169	7.442	0.0441
58	0.087	7.0605	7.087	0.0265	6.776	-0.2845	7.037	-0.0235
61	0.025	7.6021	7.242	-0.3601	7.463	-0.1391	8.294	0.6919
62	0.12	6.9208	7.302	0.3812	7.652	0.7312	7.083	0.1622
63	0.046	7.3372	6.874	-0.4632	7.197	-0.1402	6.774	-0.5632
65	0.014	7.8539	8.065	0.2111	8.028	0.1741	8.195	0.3411
67	0.016	7.7959	7.516	-0.2799	7.646	-0.1499	7.509	-0.2869
69	0.026	7.5850	8.25	0.6650	8.062	0.4770	8.05	0.4650
70	0.027	7.5686	8.464	0.8954	7.828	0.2594	7.895	0.3264
71	0.0084	8.0757	7.408	-0.6677	7.642	-0.4337	7.824	-0.2517
73	0.05	7.3010	7.843	0.5420	7.527	0.2260	7.898	0.5970
74	0.091	7.0410	7.165	0.1240	7.248	0.2070	7.006	-0.0350
76	0.015	7.8239	7.451	-0.3729	7.536	-0.2879	7.751	-0.0729
77	0.03	7.5229	7.846	0.3231	7.437	-0.0859	7.865	0.3421
81	0.049	7.3098	7.165	-0.1448	7.322	0.0122	7.221	-0.0888
86	0.87	6.0605	6.472	0.4115	6.008	-0.0525	6.291	0.2305
87	11.6	4.9355	5.97	1.0345	5.465	0.5295	5.432	0.4965
88	2.6	5.5850	5.885	0.3000	5.891	0.3060	5.959	0.3740
91	0.084	7.0757	6.678	-0.3977	6.329	-0.7467	6.657	-0.4187
92	0.16	6.7959	6.699	-0.0969	7.052	0.2561	6.792	-0.0039
93	0.12	6.9208	6.727	-0.1938	6.716	-0.2048	6.715	-0.2058
96	0.19	6.7212	6.954	0.2328	6.983	0.2618	6.67	-0.0512
98	0.95	6.0223	7.159	1.1367	7.224	1.2017	7.155	1.1327
99	0.017	7.7696	8.011	0.2414	7.636	-0.1336	8.157	0.3874
103	0.03	7.5229	7.424	-0.0989	7.431	-0.0919	7.886	0.3631
105	0.011	7.9586	7.794	-0.1646	7.822	-0.1366	7.817	-0.1416
106	0.019	7.7212	8.518	0.7968	8.232	0.5108	7.937	0.2158
107	0.0071	8.1487	7.943	-0.2057	7.745	-0.4037	7.802	-0.3467
114	0.0054	8.2676	9.048	0.7804	8.431	0.1634	8.508	0.2404
115	0.03	7.5229	9.072	1.5491	8.49	0.9671	8.559	1.0361
116	0.0074	8.1308	8.207	0.0762	8.522	0.3912	7.724	-0.4068
117	0.048	7.3188	7.621	0.3022	7.076	-0.2428	7.558	0.2392
118	0.057	7.2441	7.627	0.3829	7.284	0.0399	7.46	0.2159
121	0.11	6.9586	8.194	1.2354	7.452	0.4934	7.539	0.5804
124	0.075	7.1249	9.255	2.1301	8.968	1.8431	9.245	2.1201
126	0.24	6.6198	5.975	-0.6448	6.482	-0.1378	6.651	0.0312
128	0.76	6.1192	6.825	0.7058	7.137	1.0178	5.96	-0.1592
130	0.036	7.4437	7.384	-0.0597	7.36	-0.0837	7.656	0.2123
137	0.0099	8.0044	6.998	-1.0064	7.096	-0.9084	7.428	-0.5764
138	0.017	7.7696	9.131	1.3614	8.399	0.6294	8.794	1.0244
140	0.14	6.8539	9.737	2.8831	8.832	1.9781	6.9	0.0461
141	0.097	7.0132	7.244	0.2308	7.548	0.5348	7.604	0.5908
143	0.027	7.5686	7.956	0.3874	7.15	-0.4186	7.199	-0.3696
144	0.33	6.4815	6.732	0.2505	7.729	1.2475	7.961	1.4795
145	0.015	7.8239	7.511	-0.3129	7.698	-0.1259	7.816	-0.0079
146	0.022	7.6576	7.855	0.1974	7.727	0.0694	7.643	-0.0146
149	0.054	7.2676	7.183	-0.0846	7.256	-0.0116	7.273	0.0054
150	0.058	7.2366	6.587	-0.6496	6.947	-0.2896	6.688	-0.5486

Table 7 (Continued)

compd	IC ₅₀ (μM)	pIC ₅₀	conventional CoMFA		AOS CoMFA		CoMSIA	
			calcd	residual	calcd	residual	calcd	residual
152	0.019	7.7212	6.247	-1.4742	6.412	-1.3092	6.23	-1.4912
155	2.8	5.5528	6.8	1.2472	6.412	0.8592	5.883	0.3302
156	0.68	6.1675	7.094	0.9265	6.553	0.3855	6.006	-0.1615
159	0.3	6.5229	6.512	-0.0109	6.483	-0.0399	6.353	-0.1699
160	0.83	6.0809	6.627	0.5461	6.533	0.4521	6.141	0.0601
165	0.48	6.3188	6.175	-0.1438	6.57	0.2512	6.262	-0.0568
166	0.35	6.4559	6.227	-0.2289	5.787	-0.6689	6.203	-0.2529
167	0.014	7.8539	7.823	-0.0309	7.435	-0.4189	7.899	0.0451
168	0.31	6.5086	5.953	-0.5556	5.713	-0.7956	6.135	-0.3736
170	3.7	5.4318	5.576	0.1442	5.538	0.1062	5.301	-0.1308
172	0.73	6.1367	6.373	0.2363	5.764	-0.3727	6.33	0.1933
173	0.031	7.5086	7.59	0.0814	7.897	0.3884	7.756	0.2474
175	0.98	6.0088	5.9	-0.1088	6.277	0.2682	5.991	-0.0178
178	0.194	6.7122	6.624	-0.0882	6.591	-0.1212	7.541	0.8288



(A)



(B)

Figure 6. (A) Steric fields generated with the AOS CoMFA model based on pcDHFR inhibitory activity projected onto the Connolly surface of the pcDHFR active site. (B) Hydrophobic fields generated with the CoMSIA model based on pcDHFR inhibitory activity superposed to the binding site residues with a distance of 5.0 Å from the ligand.

6-5 ring system) falls into a sterically favorable green region. The 9-methyl group of compounds (e.g., compound **85**) with a 6-5-fused ring system falls in a sterically unfavorable yellow region, as does the one of the meta substituents on the phenyl ring. The other meta substituent on the phenyl ring falls into another sterically unfavorable yellow region. The 10-substituents also fall into a sterically unfavorable region. The *p*-chloro substituents on the phenyl ring fall into the sterically favorable region. Figure 6A shows the CoMFA steric contour plot of pcDHFR inhibitory activity projected onto the Connolly surface of the active site of pcDHFR. As shown (Figure 6A), the steric

plot is in agreement with the topology of the active site, showing yellow contours in regions of the active site with restriction against bulky substituents and green contours in regions of the active site that should accommodate additional substitution on the molecule.

As shown in Figure 4B, the electrostatic contour map for the AOS CoMFA analysis of pcDHFR inhibitory activity, the slight negatively charged 5-methyl carbon lies close to a small negative charge favorable red region, which can be explained by the fact that 5-desmethyl analogues with the more positive proton in place of the methyl are generally less active. However, replacing the methyl group with more electronegative groups such as a halogen should result in a decrease in the predicted activity. The 8-position (or 7-position for 6-5 ring systems) is close to a negative charge favorable region, indicating that an electronegative heteroatom such as a nitrogen or an oxygen in that position would have a positive effect on the inhibitory activity. For the 5,6,7,8-tetrahydroquinazolines, the 8-H falls into a positive charge favorable blue region, as does the 7-H of 5,6,7,8-tetrahydro-pyrido[2,3-*d*]-pyrimidines. The methyl group of *o*-CH₃ falls into the negative charge favorable red region. The 9-substituents fall into a positive charge favorable blue region. The 10-substituents fall into two positive charge favorable blue regions, as does the 4-chloro substituent.

The pcDHFR inhibitory activity CoMSIA electrostatic contour map is displayed in Figure 5A. There is a large positive charge favorable blue region above the bridge (atom 9 and 10) between the heterocycle and the side-chain phenyl ring, suggesting that a methyl group on one of these bridge atoms would increase the activity, especially when this bridge atom is a nitrogen (The methyl group would be more positive if it is attached to a nitrogen than a carbon). The oxygen of the *m*-methoxy on the phenyl ring falls into a negative charge favorable red region. The 10-atom (or 9-atom for 6-5 fused ring systems) on the bridge falls into a negative charge favorable red region. The methyl group of the *p*-methoxy falls into a positive charge favorable blue region. The methyl group of *o*-methoxy on the phenyl ring falls into the positive charge favorable blue region.

The hydrophobic contour map of the CoMSIA model based on the pcDHFR inhibitory activity is shown in Figure 5B, and the same contour map is superimposed onto the active site of pcDHFR (Figure 6B). A hydrophilically favorable white region encloses the upper part of the ring system, suggesting that a nitrogen in the 5-position should improve the inhibitory activity. A hydrophobic favorable yellow region is close to the 8-position, indicating that a nitrogen atom at the 8-position may decrease inhibitory activity. When superimposed onto the crystal structure, this region is found to lie close to the hydrophobic Ile33. As shown, the 9-substituent is near a hydrophobically favorable yellow region, suggesting that a methyl on the 9-position should be conducive to inhibitory activity. This hydrophobically favorable polyhedron when projected onto the pcDHFR active site is close to the hydrophobic Leu25. The two ortho substituents of the phenyl ring fall into two separate

Table 8. CoMFA Actual and Predicted Activities for rl Test Set Molecules

compd	IC ₅₀ (μM)	pIC ₅₀	conventional CoMFA		AOS CoMFA		CoMSIA	
			calcd	residual	calcd	residual	calcd	residual
2	0.0076	8.1192	6.996	-1.1232	6.88	-1.2392	7.47	-0.6492
3	0.11	6.9586	7.097	0.1384	7.506	0.5474	6.802	-0.1566
6	0.042	7.3768	6.4	-0.9768	6.618	-0.7588	6.292	-1.0848
8	0.25	6.6021	5.42	-1.1821	5.684	-0.9181	5.401	-1.2011
9	0.0296	7.5287	6.19	-1.3387	7.132	-0.3967	6.645	-0.8837
10	0.128	6.8928	5.492	-1.4008	6.269	-0.6238	5.653	-1.2398
11	0.407	6.3904	6.163	-0.2274	6.32	-0.0704	5.914	-0.4764
12	0.0174	7.7595	6.141	-1.6185	6.592	-1.1675	4.67	-3.0895
15	0.044	7.3565	7.341	-0.0155	7.326	-0.0305	6.496	-0.8605
17	0.214	6.6696	6.568	-0.1016	6.6	-0.0696	6.765	0.0954
23	0.0105	7.9788	7.453	-0.5258	7.51	-0.4688	7.801	-0.1778
25	0.28	6.5528	7.473	0.9202	6.791	0.2382	6.935	0.3822
26	0.12	6.9208	7.33	0.4092	6.704	-0.2168	6.905	-0.0158
27	2.1	5.6778	7.551	1.8732	7.303	1.6252	6.826	1.1482
28	11.8	4.9281	6.478	1.5499	6.749	1.8209	6.221	1.2929
29	1.14	5.9431	5.876	-0.0671	6.993	1.0499	6.228	0.2849
32	6.1	5.2147	6.187	0.9723	6.945	1.7303	5.631	0.4163
38	59.3	4.2269	5.248	1.0211	5.132	0.9051	4.547	0.3201
39	116	3.9355	4.45	0.5145	4.137	0.2015	4.338	0.4025
40	23	4.6383	4.54	-0.0983	5.063	0.4247	4.771	0.1327
41	12	4.9208	5.181	0.2602	4.679	-0.2418	4.756	-0.1648
42	36.5	4.4377	5.156	0.7183	5.009	0.5713	5.378	0.9403
45	14.6	4.8356	5.61	0.7744	5.493	0.6574	5.488	0.6524
48	0.054	7.2676	6.288	-0.9796	6.929	-0.3386	6.63	-0.6376
49	0.21	6.6778	6.182	-0.4958	7.798	1.1202	6.825	0.1472
50	0.06	7.2218	6.769	-0.4528	7.251	0.0292	6.988	-0.2338
53	0.42	6.3768	6.091	-0.2858	6.448	0.0712	5.983	-0.3938
54	0.14	6.8539	6.35	-0.5039	6.706	-0.1479	6.377	-0.4769
59	0.082	7.0862	6.034	-1.0522	6.659	-0.4272	6.928	-0.1582
61	0.05	7.3010	6.341	-0.9600	6.702	-0.5990	7.015	-0.2860
62	0.28	6.5528	5.453	-1.0998	6.091	-0.4618	5.658	-0.8948
63	0.57	6.2441	6.195	-0.0491	6.555	0.3109	6.978	0.7339
64	0.0027	8.5686	7.722	-0.8466	8.024	-0.5446	7.623	-0.9456
68	0.0073	8.1367	6.587	-1.5497	7.6	-0.5367	7.2	-0.9367
69	0.12	6.9208	6.973	0.0522	7.375	0.4542	6.834	-0.0868
70	0.017	7.7696	7.964	0.1944	8.102	0.3324	7.041	-0.7286
71	0.024	7.6198	6.582	-1.0378	7.537	-0.0828	7.334	-0.2858
72	0.087	7.0605	7.378	0.3175	7.541	0.4805	7.707	0.6465
74	0.2	6.6990	6.221	-0.4780	7.026	0.3270	6.769	0.0700
75	0.047	7.3279	6.637	-0.6909	6.945	-0.3829	7.484	0.1561
81	0.16	6.7959	6.031	-0.7649	7.709	0.9131	6.593	-0.2029
83	0.04	7.3979	6.19	-1.2079	7.122	-0.2759	6.437	-0.9609
86	8.2	5.0862	6.101	1.0148	5.981	0.8948	5.326	0.2398
89	3	5.5229	4.536	-0.9869	5.522	-0.0009	4.584	-0.9389
90	82.9	4.0814	4.889	0.8076	5.335	1.2536	4.876	0.7946
92	1.1	5.9586	5.73	-0.2286	6.002	0.0434	5.81	-0.1486
93	0.84	6.0757	5.89	-0.1857	6.282	0.2063	6.221	0.1453
96	1.3	5.8861	5.786	-0.1001	5.879	-0.0071	5.805	-0.0811
98	22.7	4.6440	6.33	1.6860	6.304	1.6600	5.7	1.0560
100	0.19	6.7212	6.298	-0.4232	6.707	-0.0142	6.388	-0.3332
102	0.017	7.7696	6.563	-1.2066	7.367	-0.4026	7.3	-0.4696
103	0.026	7.5850	6.477	-1.1080	6.942	-0.6430	6.657	-0.9280
105	0.037	7.4318	6.328	-1.1038	6.911	-0.5208	7.404	-0.0278
107	0.088	7.0555	6.835	-0.2205	7.928	0.8725	7.505	0.4495
108	0.0556	7.2549	7.171	-0.0839	7.984	0.7291	7.861	0.6061
110	0.0349	7.4572	6.498	-0.9592	6.856	-0.6012	6.933	-0.5242
112	0.018	7.7447	6.338	-1.4067	6.818	-0.9267	7.521	-0.2237
113	0.17	6.7696	6.948	0.1784	6.989	0.2194	6.842	0.0724
117	0.15	6.8239	6.42	-0.4039	7.224	0.4001	6.109	-0.7149
120	0.47	6.3279	6.48	0.1521	6.65	0.3221	7.389	1.0611
122	0.23	6.6383	8.047	1.4087	7.782	1.1437	7.688	1.0497
124	0.17	6.7696	7.681	0.9114	8.076	1.3064	7.98	1.2104
126	1.12	5.9508	5.337	-0.6138	6.668	0.7172	6.21	0.2592
129	0.16	6.7959	5.933	-0.8629	5.602	-1.1939	5.933	-0.8629
131	0.047	7.3279	7.212	-0.1159	7.219	-0.1089	7.387	0.0591
133	0.15	6.8239	7.534	0.7101	6.729	-0.0949	6.967	0.1431
136	0.227	6.6440	6.909	0.2650	6.749	0.1050	6.681	0.0370
140	1.47	5.8327	7.799	1.9663	7.108	1.2753	5.56	-0.2727
141	0.24	6.6198	7.108	0.4882	6.733	0.1132	7.192	0.5722
142	0.128	6.8928	7.402	0.5092	6.506	-0.3868	6.514	-0.3788
143	0.16	6.7959	6.46	-0.3359	5.46	-1.3359	6.523	-0.2729
145	0.26	6.5850	6.886	0.3010	6.996	0.4110	7.054	0.4690
148	0.074	7.1308	6.17	-0.9608	6.547	-0.5838	6.776	-0.3548
149	0.29	6.5376	6.306	-0.2316	5.99	-0.5476	6.648	0.1104
150	0.23	6.6383	5.579	-1.0593	6.524	-0.1143	6.148	-0.4903

Table 8 (Continued)

compd	IC ₅₀ (μM)	pIC ₅₀	conventional CoMFA		AOS CoMFA		CoMSIA	
			calcd	residual	calcd	residual	calcd	residual
152	0.018	7.7447	5.657	-2.0877	6.095	-1.6497	6.713	-1.0317
155	3.8	5.4202	5.837	0.4168	6.914	1.4938	6.185	0.7648
156	1.1	5.9586	6.205	0.2464	6.524	0.5654	6.038	0.0794
158	3.2	5.4949	5.747	0.2521	6.551	1.0561	5.742	0.2471
159	0.43	6.3665	5.947	-0.4195	6.285	-0.0815	6.304	-0.0625
165	1.1	5.9586	5.026	-0.9326	5.831	-0.1276	5.753	-0.2056
166	3.3	5.4815	5.428	-0.0535	5.303	-0.1785	5.867	0.3855
167	0.033	7.4815	7.193	-0.2885	7.036	-0.4455	7.566	0.0845
168	0.35	6.4559	5.417	-1.0389	5.818	-0.6379	5.429	-1.0269
170	2.9	5.5376	6.675	1.1374	5.891	0.3534	6.147	0.6094
172	1.5	5.8239	5.484	-0.3399	5.333	-0.4909	6.337	0.5131
173	0.072	7.1427	6.791	-0.3517	7.526	0.3833	7.309	0.1663
175	0.24	6.6198	5.941	-0.6788	6.794	0.1742	6.362	-0.2578
178	1.27	5.8962	6.811	0.9148	5.785	-0.1112	7.151	1.2548

hydrophilic white regions, respectively, indicating that the importance of polar oxygens in the form of methoxy groups at these positions should improve inhibitory activity. One of these regions is close to the hydrophilic Ser64 in the active site, while the other lies in a hydrophobic pocket composed of Phe36, Leu72, and Ile123. This apparent discrepancy is probably due to the inappropriate orientation of the 2-OMe-phenyl moiety when the compounds were flexible-aligned with the template compound **1**, which has no methoxy substituents on the phenyl ring but rather a 2-naphthyl in place of the phenyl ring. A large hydrophobic favorable yellow region near Phe69 in the active site is found to be close to the phenyl ring that could be reached by a naphthyl group.

As revealed in the steric contours of the AOS CoMFA analysis for tgDHFR inhibition (Figure 4C), the 5-methyl group of a 6-6 fused ring system is in contact with both a sterically favorable green region and a sterically unfavorable yellow region manifesting the important yet subtle role the 5-methyl plays in tgDHFR inhibitory activity. The 9-substituents (or 8-substituents for 6-5 fused ring systems) fall into the same sterically favorable region as well, suggesting that a methyl group at that position should be favorable for inhibitory activity. The ortho substituents of the phenyl ring fall into a sterically unfavorable yellow region. The meta substituents of the phenyl ring also fall into another sterically unfavorable yellow region. The *p*-methoxy oxygen falls into the sterically favorable green region; however, the methyl group of *p*-OCH₃ falls into the sterically unfavorable yellow region, indicating that a single-atom substituent (e.g., a chloro) at that position is optimal for activity.

The electrostatic field constructed on the basis of the CoMFA analysis for tgDHFR inhibitory activity is shown in Figure 4D. The 5-methyl falls into the negative charge favorable red region. As in the case of pcDHFR inhibitory activity analysis, since the carbon of this methyl group is slightly negatively charged, the existence of the red region is simply due to the fact that a compound with a 5-methyl is generally more potent. The 9-substituents fall into a positive charge favorable blue region, which again suggests that a methyl group as the 9-substituent would be beneficial to inhibitory activity. The *m*- and *o*-chloro groups fall into a negative charge favorable red region, as does the *p*-chloro group. Both the *m*-OCH₃ and the *β*-OCH₃ methyl fall into a positive charged favorable blue region. Thus, the contour maps near the phenyl moiety suggest that both methoxy and chloro substituents would contribute positively to the inhibitory activity.

Contrary to pcDHFR, a large negative charge favorable region is found above the bridge in the CoMSIA electrostatic map for tgDHFR inhibitory activity (Figure 5C), revealing that a 9- or 10-methyl is unfavorable to the inhibitory activity. There is a positive charge favorable blue region near the 8-position of the ring system, indicating that a nitrogen in this position should not improve the inhibitory activity. The 10-substituent (or 9-substituents for 6-5 fused ring systems) falls into a positive charged favorable blue region, as do the ortho substituents on the phenyl ring.

Figure 5D is the orthogonal view of the hydrophobic contour map from the CoMSIA analysis for tgDHFR inhibitory activity. The 5-methyl is in contact with two discrete hydrophobic favorable yellow regions. A hydrophilic favorable white region encloses the upper right-hand side of the ring system. A hydrophobic favorable yellow region is found near the 8-position (or 7-position for a 6-5 fused ring system). The 10-substituents (or 9-substituents for a 6-5 fused ring system) fall into a hydrophobic favorable yellow region. The methyl of the *m*-methoxy is also near a hydrophobic favorable yellow region, while the *m*-chloro falls into a hydrophilic favorable white region.

The AOS CoMFA analysis for rat liver DHFR inhibition was used in the construction of the steric contour map (Figure 4E). The 5-methyl group of the 6-6 fused ring system is in contact with both a sterically favorable green region and a sterically unfavorable yellow region. A sterically favorable green region is also found near the 10-substituent. Sterically unfavorable yellow regions were found near the meta and para substituents on the phenyl ring.

Similar to the pcDHFR and tgDHFR analyses, the 5-methyl group falls into a negative charge favorable red region in the electrostatic contour of rIDHFR AOS CoMFA analysis (Figure 4F). The 10-methyl group falls into a positive charge favorable blue region. The *m*-methoxy group falls into the positive charge favorable blue region. The *o*-chloro falls into the positive charge favorable blue region as do the *m*-methoxy and *p*-methoxy groups.

As shown in the CoMSIA electrostatic contours from the rIDHFR (Figure 5E). A negative charge favorable red region was found near the 5-position. The 10-substituents fall into a positive charge favorable blue region. Another negative charge favorable red region was found near the 10-position, while the *m*-methoxy oxygen is close to a negative charge favorable red region. The ortho substituents on the phenyl ring fall into a positive charge favorable blue region.

The CoMSIA hydrophobic contour map of rat liver DHFR inhibition (Figure 5F) is very close to that of the pcDHFR except for the hydrophilic favorable white region near the phenyl ring which is near the para substituents rather than the ortho substituents for pcDHFR.

Summary and Conclusion

We have investigated the 3D QSAR of pcDHFR, tgDHFR, and rIDHFR. Predictive AOS CoMFA and CoMSIA models were developed for the inhibition against these enzymes using 90-compound test sets taken from a data set of 179 compounds. Each model was validated by using an external test set of 89 compounds not included in its training set. Best internal predictions measured by the q^2 were obtained with AOS CoMFA models ($q^2 = 0.604, 0.600, \text{ and } 0.634$ for pcDHFR, tgDHFR, and rat liver DHFR respectively),

whereas the best external predictions measured by the predictive r^2 were obtained with the CoMSIA models (predictive $r^2 = 0.544, 0.648, \text{ and } 0.488$ for pcDHFR, tgDHFR, and rat liver DHFR respectively). These statistical data are satisfactory. AOS CoMFA and CoMSIA 3D maps obtained from the analyses can be used for the design of new inhibitors in an interactive fashion.

Acknowledgment. We thank Dr. Barbra Laughon from NIAID for providing the inhibitory data in a usable form. This work was supported in part by the National Institutes of Health, National Institute of Allergy and Infectious Diseases AI047759 (A.G.).

References

- Masur, H. Problems in the Management of Opportunistic Infections in Patients Infected with Human Immunodeficiency Virus. *J. Infect. Dis.* **1990**, *161*, 858–864.
- Masur, H. Prevention and Treatment of Pneumocystis Pneumonia. *N. Engl. J. Med.* **1992**, *327*, 1853–1860.
- Dannemann, B.; McCutchan, J.; Israeleki, A. D. Treatment of Toxoplasmic Encephalitis in Patients with AIDS. A Randomized Trial Comparing Pyrimethamine plus Clindamycin to Pyrimethamine plus Sulfadiazine. The California Collaborative Treatment Group. *Ann. Intern. Med.* **1992**, *116*, 33–43.
- Gangjee, A.; Adair, O.; Queener, S. F. *Pneumocystis carinii* and *Toxoplasma gondii* Dihydrofolate Reductase Inhibitors and Antitumor Agents: Synthesis and Biological Activities of 2,4-Diamino-5-methyl-6-[(monosubstituted anilino)methyl]-pyrido-[2,3-d]pyrimidines. *J. Med. Chem.* **1999**, *42*, 2447–2455.
- Piper, J. R.; Johnson, C. A.; Krauth, C. A.; Carter, R. L.; Hosmer, C. A.; Queener, S. F.; Borotz, S. E.; Pfefferkorn, E. R. Lipophilic Antifolates as Agents against Opportunistic Infections. I. Agents Superior to Trimetrexate and Piritrexim against *Toxoplasma gondii* and *Pneumocystis carinii* in *in Vitro* Evaluations. *J. Med. Chem.* **1996**, *39*, 1271–1280.
- Rosowsky, A.; Cody, V.; Galitsky, N.; Fu, H.; Papoulis, A. T.; Queener, S. F. Structure-based Design of Selective Inhibitors of Dihydrofolate Reductase: Synthesis and Antiparasitic Activity of 2,4-Diaminopteridine Analogues with a Bridged Diarylamine Side Chain. *J. Med. Chem.* **1999**, *42*, 4853–4860.
- Stevens, M. F. G.; Phillip, K. S.; Rathbone, D. L.; O'Shea, D. M.; Queener, S. F.; Schwalbe, C. H.; Lambert, P. A. Structural Studies on Bioactive Compounds. 28. Selective Activity of Triazenyloxy-substituted Pyrimethamine Derivatives against *Pneumocystis carinii* Dihydrofolate Reductase. *J. Med. Chem.* **1997**, *40*, 1886–1893.
- Ivanciuc, O.; Ivanciuc, T.; Cabrol-Bass, D. QSAR for Dihydrofolate Reductase Inhibitors with Molecular Graph Structural Descriptors. *Theochem. J. Mol. Struct.* **2002**, *582*, 39–51.
- Burbridge, R.; Trotter, M.; Buxton, B.; Holden, S. Drug Design by Machine Learning: Support Vector Machines for Pharmaceutical Data Analysis. *Comput. Chem.* **2001**, *26*, 5–14.
- S. Garg, L. E. K. Achenie, Mathematical Programming Assisted Drug Design for Nonclassical Antifolates. *Biotechnol. Prog.* **2001**, *17*, 412–418.
- Zheng, W.; Tropsha, A. Novel Variable Selection Quantitative Structure–property Relationship Approach Based on the K-nearest Neighbor Principle. *J. Chem. Inf. Comput. Sci.* **2000**, *40*, 185–194.
- Selassie, C. D.; Gan, W.-X.; Kallander, L. S.; Klein, T. E. Quantitative Structure–activity Relationships of 2,4-Diamino-5-(2-X-benzyl)pyrimidines versus Bacterial and Avian Dihydrofolate Reductase. *J. Med. Chem.* **1998**, *41*, 4261–4272.
- Burden, F. R.; Rosewarne, B. S.; Winkler, D. A. Predicting Maximum Bioactivity by Effective Inversion of Neural Networks Using Genetic Algorithms. *Chemom. Intell. Lab. Syst.* **1997**, *38*, 127–137.
- Kyngas, J.; Valjakka, J. Evolutionary Neural Networks in Quantitative Structure–activity Relationships of Dihydrofolate Reductase Inhibitors. *Quant. Struct.-Act. Relat.* **1996**, *15*, 296–301.
- Ivanciuc, O. Artificial Neural Networks Applications. Part 2. Using Theoretical Descriptors of Molecular Structure in Quantitative Structure–activity Relationships: Analysis of the Inhibition of Dihydrofolate Reductase. *Rev. Roum. Chim.* **1996**, *41*, 645–652.
- Marlowe, C. K.; Selassie, C. K.; Santi, D. V. Quantitative Structure–Activity Relationships of the Inhibition of *Pneumocystis carinii* Dihydrofolate Reductase by 4,6-Diamino-1,2-dihydro-2,2-dimethyl-1-(X-phenyl)-s-triazines. *J. Med. Chem.* **1995**, *38*, 967–972.
- Hirst, J. D.; King, R. D.; Sternberg, M. J. E. Quantitative Structure–activity Relationships by Neural Networks and Inductive Logic Programming. II. The Inhibition of Dihydrofolate Reductase by Triazines. *J. Comput.-Aided Mol. Des.* **1994**, *8*, 421–432.
- Hirst, J. D.; King, R. D.; Sternberg, M. J. E. Quantitative Structure–activity Relationships by Neural Networks and Inductive Logic Programming. I. The Inhibition of Dihydrofolate Reductase by Pyrimidines. *J. Comput.-Aided Mol. Des.* **1994**, *8*, 405–420.
- Stanton, D. T.; Murray, W. J.; Jurs, P. C. Comparison of QSAR and Molecular Similarity Approaches for a Structure–activity Relationship Study of DHFR Inhibitors. *Quant. Struct.-Act. Relat.* **1993**, *12*, 239–245.
- So, S.-S.; Richards, W. G. Application of Neural Networks: Quantitative Structure–Activity Relationships of the Derivatives of 2,4-Diamino-5-(substituted-benzyl)pyrimidines as DHFR Inhibitors. *J. Med. Chem.* **1992**, *35*, 3201–3207.
- Selassie, C. D.; Li, R.-L.; Poe, M.; Hansch, C. On the Optimization of Hydrophobic and Hydrophilic Substituent Interactions of 2,4-Diamino-5-(substituted-benzyl)pyrimidines with Dihydrofolate Reductase. *J. Med. Chem.* **1991**, *34*, 46–54.
- Debnath, A. K.; Lopez de Compadre, R. L.; Debnath, G.; Shusterman, A. J.; Hansch, C. Structure–Activity Relationship of Mutagenic Aromatic and Heteroaromatic Nitro Compounds: Correlation with Molecular Orbital Energies and Hydrophobicity. *J. Med. Chem.* **1991**, *34*, 786–797.
- Andrea, T. A.; Kalayeh, H. Applications of Neural Networks in Quantitative Structure–Activity Relationships of Dihydrofolate Reductase Inhibitors. *J. Med. Chem.* **1991**, *34*, 2824–2836.
- Selassie, C. D.; Fang, Z.-X.; Li, R.-L.; Hansch, C.; Debnath, G.; Klein, T. E.; Langridge, R.; Kaufman, B. T. On the Structure Selectivity Problem in Drug Design: A Comparative Study of Benzylpyrimidine Inhibition of Vertebrate and Bacterial Dihydrofolate Reductase via Molecular Graphics and Quantitative Structure–Activity Relationships. *J. Med. Chem.* **1989**, *32*, 1895–1905.
- Li, R.-L.; Poe, M. Quantitative Structure–Activity Relationships for the Inhibition of *Escherichia coli* Dihydrofolate Reductase by 5-(Substituted benzyl)-2,4-diaminopyrimidines. *J. Med. Chem.* **1988**, *31*, 366–370.
- Booth, R. G.; Selassie, C. D.; Hansch, C.; Santi, D. V. Quantitative Structure–Activity Relationship of Triazine-antifolate Inhibition of *Leishmania* Dihydrofolate Reductase and Cell Growth. *J. Med. Chem.* **1987**, *30*, 1218–1224.
- Selassie, C. D.; Fang, Z.-X.; Li, R.-L.; Hansch, C.; Klein, T. E.; Langridge, R.; Kaufman, B. T. Inhibition of Chicken Liver Dihydrofolate Reductase by 5-(Substituted benzyl)-2,4-diaminopyrimidines: A Quantitative Structure–Activity Relationship and Graphics Analysis. *J. Med. Chem.* **1986**, *29*, 621–626.
- Ghose, A. K.; Crippen, G. M. Use of Physicochemical Parameters in Distance Geometry and Related Three-Dimensional Quantitative Structure–Activity Relationships: A Demonstration Using *Escherichia coli* Dihydrofolate Reductase Inhibitors. *J. Med. Chem.* **1985**, *28*, 333–346.
- Hansch, C.; Hathaway, B. A.; Guo, Z.-R.; Selassie, C. D.; Dietrich, S. W.; Blaney, J. M.; Langridge, R.; Volz, K. W.; Kaufman, B. T. Crystallography, Quantitative Structure–Activity Relationships, and Molecular Graphics in a Comparative Analysis of the Inhibition of Dihydrofolate Reductase from Chicken Liver and *Lactobacillus casei* by 4,6-Diamino-1,2-dihydro-2,2-dimethyl-1-(substituted-phenyl)-s-triazines. *J. Med. Chem.* **1984**, *27*, 129–143.
- Hathaway, B. A.; Guo, Z.-R.; Hansch, C.; Delcamp, T. J.; Susten, S. S.; Freisheim, J. H. Inhibition of Human Dihydrofolate Reductase by 4,6-Diamino-1,2-dihydro-2,2-dimethyl-1-(substituted-phenyl)-s-triazines: A Quantitative Structure–Activity Relationship Analysis. *J. Med. Chem.* **1984**, *27*, 144–149.
- Hopfinger, A. J. Theory and Application of Molecular Potential Energy Fields in Molecular Shape Analysis: A Quantitative Structure–Activity Relationship Study of 2,4-Diamino-5-Benzylpyrimidines as Dihydrofolate Reductase Inhibitors. *J. Med. Chem.* **1983**, *26*, 990–996.
- Khawaja, T. A.; Pentecost, S.; Selassie, C. D.; Guo, Z.-R.; Hansch, C. Comparison of Quantitative Structure–Activity Relationships of the Inhibition of Leukemia Cells in Culture with the Inhibition of Dihydrofolate Reductase from Leukemia Cells and Other Cell Types. *J. Med. Chem.* **1982**, *25*, 153–156.
- Hansch, C.; Li, R.-L.; Blaney, J. M.; Langridge, R. Comparison of the Inhibition of *Escherichia coli* and *Lactobacillus casei* Dihydrofolate Reductase by 2,4-Diamino-5-(substituted-benzyl)pyrimidines: Quantitative Structure–Activity Relationships, X-ray Crystallography, and Computer Graphics in Structure–Activity Analysis. *J. Med. Chem.* **1982**, *25*, 777–784.
- Ghose, A. K.; Crippen, G. M. Quantitative Structure–Activity Relationship by Distance Geometry: Quinazolines as Dihydrofolate Reductase Inhibitors. *J. Med. Chem.* **1982**, *25*, 892–899.

- (35) Li, R.-L.; Dietrich, S. W.; Hansch, C. Quantitative Structure–Selectivity Relationships. Comparison of the Inhibition of *Escherichia coli* and Bovine Liver Dihydrofolate Reductase by 5-(Substituted-benzyl)-2,4-diaminopyrimidines. *J. Med. Chem.* **1981**, *24*, 538–544.
- (36) Coats, E. A.; Genther, C. S.; Dietrich, S. W.; Guo, Z.-R.; Hansch, C. Comparison of the Inhibition of Methotrexate-Sensitive and -Resistant *Lactobacillus casei* Cell Cultures with Purified *Lactobacillus casei* Dihydrofolate Reductase by 4,6-Diamino-1,2-dihydro-2,2-dimethyl-1-(3-substituted-phenyl)-s-triazines: Use of Quantitative Structure–Activity Relationships in Making Inferences about the Mechanism of Resistance and the Structure of the Enzyme in Situ Compared with the Enzyme in Vitro. *J. Med. Chem.* **1981**, *24*, 1422–1429.
- (37) Crippen, G. M. Quantitative Structure–Activity Relationships by Distance Geometry: Systematic Analysis of Dihydrofolate Reductase Inhibitors. *J. Med. Chem.* **1980**, *23*, 599–606.
- (38) Dietrich, S. W.; Blaney, J. M.; Reynolds, M. A.; Jow, P. Y. C.; Hansch, C. Quantitative Structure–Selectivity Relationships. Comparison of the Inhibition of *Escherichia coli* and Bovine Liver Dihydrofolate Reductase by 5-(Substituted-benzyl)-2,4-diaminopyrimidines. *J. Med. Chem.* **1980**, *23*, 1205–1212.
- (39) Blaney, J. M.; Hansch, C.; Silipo, C.; Vittoria, A. Structure–Activity Relationships of Dihydrofolate Reductase Inhibitors. *Chem. Rev.* **1984**, *84*, 333–407.
- (40) Mattioni, B. E.; Jurs, P. C. Prediction of Dihydrofolate Reductase Inhibition and Selectivity Using Computational Neural Networks and Linear Discriminant Analysis. *J. Mol. Graphics Modell.* **2003**, *21*, 391–419.
- (41) Gangjee, A.; Shi, J.; Queener, S. F.; Barrows, L.; Kisliuk, R. L. Synthesis of 5-Methyl-5-deaza Nonclassical Antifolates as Inhibitors of Dihydrofolate Reductases and as Potential Antipneumocystis, Antitoxoplasma, and Antitumor Agents. *J. Med. Chem.* **1993**, *36*, 3437–3443.
- (42) Gangjee, A.; Devraj, R.; Queener, S. F. Synthesis and Dihydrofolate Reductase Inhibitory Activities of 2,4-Diamino-5-deaza and 2,4-Diamino-5,10-dideaza Lipophilic Antifolates. *J. Med. Chem.* **1997**, *40*, 470–478.
- (43) Gangjee, A.; Mavandadi, F.; Queener, S. F.; McGuire, J. J. Novel 2,4-Diamino-5-Substituted-pyrrolo[2,3-*d*]pyrimidines as Classical and Nonclassical Antifolate Inhibitors of Dihydrofolate Reductases. *J. Med. Chem.* **1995**, *38*, 2158–2165.
- (44) Gangjee, A.; Guo, X.; Queener, S. F.; Cody, V.; Galitsky, N.; Luft, J. R.; Pangborn, W. Selective *Pneumocystis carinii* Dihydrofolate Reductase Inhibitors: Design, Synthesis, and Biological Evaluation of New 2,4-Diamino-5-substituted-furo[2,3-*d*]pyrimidines. *J. Med. Chem.* **1998**, *41*, 1263–1271.
- (45) Gangjee, A.; Zhu, Y.; Queener, S. F.; Francom, P.; Broom, A. D. Nonclassical 2,4-Diamino-8-deazafolate Analogues as Inhibitors of Dihydrofolate Reductases from Rat Liver, *Pneumocystis carinii*, and *Toxoplasma gondii*. *J. Med. Chem.* **1996**, *39*, 1836–1845.
- (46) Gangjee, A.; Mavandadi, F.; Queener, S. F. Effect of N9-Methylation and Bridge Atom Variation on the Activity of 5-Substituted 2,4-Diaminopyrrolo[2,3-*d*]pyrimidines against Dihydrofolate Reductases from *Pneumocystis carinii* and *Toxoplasma gondii*. *J. Med. Chem.* **1997**, *40*, 1173–1177.
- (47) Gangjee, A.; Vidwans, A. P.; Vasudevan, A.; Queener, S. F.; Kisliuk, R. L.; Cody, V.; Li, R.; Galitsky, N.; Luft, J. R.; Pangborn, W. Structure-Based Design and Synthesis of Lipophilic 2,4-Diamino-6-Substituted Quinazolines and Their Evaluation as Inhibitors of Dihydrofolate Reductases and Potential Antitumor Agents. *J. Med. Chem.* **1998**, *41*, 3426–3434.
- (48) Gangjee, A.; Adair, O.; Queener, S. F. *Pneumocystis carinii* and *Toxoplasma gondii* Dihydrofolate Reductase Inhibitors and Antitumor Agents: Synthesis and Biological Activities of 2,4-Diamino-5-methyl-6-(monosubstituted anilino)methylpyrido[2,3-*d*]pyrimidines. *J. Med. Chem.* **1999**, *42*, 2447–2455.
- (49) Gangjee, A.; Vasudevan, A.; Queener, S. F. Synthesis and Biological Evaluation of Nonclassical 2,4-Diamino-5-methylpyrido[2,3-*d*]pyrimidines with Novel Side Chain Substituents as Potential Inhibitors of Dihydrofolate Reductases. *J. Med. Chem.* **1997**, *40*, 479–485.
- (50) Gangjee, A.; Shi, J.; Queener, S. F. Synthesis and Biological Activities of Conformationally Restricted, Tricyclic Nonclassical Antifolates as Inhibitors of Dihydrofolate Reductases. *J. Med. Chem.* **1997**, *40*, 1930–1936.
- (51) Gangjee, A.; Zaveri, N.; Kothare, M.; Queener, S. F. Nonclassical 2,4-Diamino-6-(aminomethyl)-5,6,7,8-tetrahydroquinazoline Antifolates: Synthesis and Biological Activities. *J. Med. Chem.* **1995**, *38*, 3660–3668.
- (52) Gangjee, A.; Zhu, Y.; Queener, S. F. 6-Substituted 2,4-Diaminopyrido[3,2-*d*]pyrimidine Analogues of Piritrexim as Inhibitors of Dihydrofolate Reductase from Rat Liver, *Pneumocystis carinii*, and *Toxoplasma gondii* and as Antitumor Agents. *J. Med. Chem.* **1998**, *41*, 4533–4541.
- (53) Gangjee, A.; Vasudevan, A.; Queener, S. F.; Kisliuk, R. L. 2,4-Diamino-5-deaza-6-Substituted Pyrido[2,3-*d*]pyrimidine Antifolates as Potent and Selective Nonclassical Inhibitors of Dihydrofolate Reductases. *J. Med. Chem.* **1996**, *39*, 1438–1446.
- (54) Wang, R.; Gao, Y.; Liu, L.; Lai, L. All-Orientation Search and All-Placement Search in Comparative Molecular Field Analysis. *J. Mol. Model.* **1998**, *4*, 276–283.
- (55) Labute, P.; Williams, C. Flexible Alignment of Small Molecules. *J. Med. Chem.* **2001**, *44*, 1483–1490.
- (56) Molecular Operating Environment (MOE 2002.03), Chemical Computing Group, Inc, 1255 University St., Suite 1600, Montreal, Quebec, Canada, H3B 3X3.
- (57) SYBYL Version 6.7 10, 2000; Tripos Associates: St. Louis, MO.
- (58) Cho, S. J.; Tropsha, A. Cross-Validated R2-Guided Region Selection for Comparative Molecular Field Analysis: A Simple Method To Achieve Consistent Results. *J. Med. Chem.* **1995**, *38*, 1060–1066.
- (59) Klebe, G.; Abraham, U.; Mietzner, T. Molecular Similarity Indices in a Comparative Analysis (CoMSIA) of Drug Molecules to Correlate and Predict Their Biological Activity. *J. Med. Chem.* **1994**, *37*, 4130–4146.
- (60) Viswanadhan, V. N.; Ghose, A. K.; Revankar, G. R.; Robins, R. K. Atomic Physicochemical Parameters for Three Dimensional Structure Directed Quantitative Structure–Activity Relationships. 4. Additional Parameters for Hydrophobic and Dispersive Interactions and Their Application for an Automated Superposition of Certain Naturally Occurring Nucleoside Antibiotics. *J. Chem. Inf. Comput. Sci.* **1989**, *29*, 163–172.
- (61) Klebe, G. The Use of Composite Crystal-field Environments in Molecular Recognition and the de novo Design of Protein Ligands. *J. Mol. Biol.* **1994**, *237*, 212–235.